Calibration of response amplitude operators based on measurements of vessel motions and directional wave spectra

Skandali, D.; Lourens, E.; Ogink, R.

DOI
10.1016/j.marstruc.2020.102774

Publication date
2020

Document Version
Accepted author manuscript

Published in
Marine Structures

Citation (APA)
Skandali, D., Lourens, E., & Ogink, R. (2020). Calibration of response amplitude operators based on measurements of vessel motions and directional wave spectra. *Marine Structures*, *72*, Article 102774. https://doi.org/10.1016/j.marstruc.2020.102774

Calibration of Response Amplitude Operators based on Measurements of Vessel Motions and Directional Wave Spectra

D. Skandali[1,2], E. Lourens[1], R.H.M. Ogink[1,2]

[1]Faculty of Civil Engineering and Geosciences, Delft University of Technology, Delft, The Netherlands

[2]Heerema Marine Contractors Nederland SE, Leiden, The Netherlands

Abstract

A vessel's response to waves is dependent on a large number of parameters, some of which are both frequency and direction dependent. To predict vessel response, these parameters are used to construct response amplitude operators (RAOs) that act as transfer functions between the directional wave spectra and the motion spectra of the vessel. In particular situations, however, vessel motions predicted using RAOs calculated with general-purpose radiation-diffraction codes and measured wave spectra are found to deviate from measured vessel responses. To address this problem, a methodology for calibrating RAOs based on measurements of the directional wave spectra and vessel motions is proposed. Use is made of a vector fitting method through which the frequency dependent hydrodynamic properties of the vessel can be approximated by a ratio of two polynomials, thus greatly reducing the number of parameters that need to be calibrated. The reduced set of parameters is subsequently related to previously identified causes of RAO inaccuracy in order to arrive at optimization algorithms for identifying more accurate RAOs from the measurements. It is shown that the RAOs can be improved with accuracy in situations where the discrepancies are caused by imprecise estimates for the vessel's radii of gyration, center of gravity, or viscous damping. When the discrepancies in the RAOs are related to the potential mass, damping and wave forces, however, the problem becomes highly non-convex and it is not possible to find a unique RAO that satisfies the data.

Keywords: response amplitude operator, vector fitting, directional wave spectra, vessel motion, calibration procedure

1 INTRODUCTION

Accurate prediction of ship, barge or semi-submersible motion during offshore projects is of importance to the operator of the vessel. A vessel's motion response to incoming waves is calculated on the basis of Response Amplitude Operators (RAOs). The incoming irregular waves are described by frequency- and direction-dependent wave spectra. The vessel's response spectra are then calculated by multiplying the wave spectra by the RAOs squared. In the offshore industry, these RAOs are typically calculated using general-purpose radiation-diffraction codes [1, 2]. These codes are based on two- or three-dimensional analyses that predict linear wave induced loads on large volume structures [1, 2, 3, 4, 5] on the basis of potential theory.

To verify the accuracy of the calculations, the vessel motions can be measured by, for example, Motion Reference Units (MRUs). In particular cases, the measured vessel motions are found to differ from the predicted (calculated) motions. Inaccuracies have, among others, been observed in the following cases:

- A semi-submersible vessel on a draught with a small amount of water on the floaters: the so-called inconvenient draught.
- When viscous damping forces are of the same order of magnitude or even larger than potential damping forces due to wave radiation.
- When the mass distribution or the centre of gravity (CoG) of the vessel changes.

Diffraction software is less reliable for calculation of RAOs for semi-submersibles with a thin layer of water on the floater. The standing wave pattern that develops on the floaters and the breaking of those waves is predicted incorrectly by conventional diffraction theory, resulting in incorrect wave radiation and diffraction potentials. Matters are complicated even further, if the floaters emerge and re-submerge. This results in a non-constant water plane area and therefore in non-constant restoring forces in the motion equations. Calculation of RAOs for semi-submersibles at inconvenient draught with CFD is ongoing research within the offshore industry [6, 7, 8].

Viscous damping forces due to eddy shedding can be as large as or even larger than the potential damping forces. Depending on the hull shape, this is especially true for roll damping. This means that for accurate roll prediction, a viscous damping force has to be added to the potential forces in the equations of motion [3, 9]. Estimates for viscous roll damping of monohulls are often based on the work of Tanaka [10]. An example of the evaluation of the viscous roll damping of a semi-submersible is given in [22]. A recent overview of prediction methods for roll damping of ships is given in [11].

During offshore projects the mass distribution of vessels can change, for example when heavy loads are shifted on the vessel or are transferred from vessel to vessel. This can result in situations in which the CoG and/or the radii of gyration of the vessel are not known accurately. Also more generally, fuel consumption will change the mass distribution of the vessel as well. Incomplete knowledge of the mass distribution will result in inaccurate RAO determination.

The phenomena mentioned above can result in inaccurate motion prediction when standard RAOs are used. Often during offshore installation projects, frequency- and direction-dependent wave spectra are recorded by special purpose buoys and the vessel motions are recorded by MRUs. The difficulty in back-calculation of the RAOs lies in the measured wave spectra having wave energy over multiple directions. RAOs need to be determined for each combination of vessel Degree of Freedom (DoF) and incoming wave direction. Each incoming wave direction transfers energy to each of the 6 vessel DoFs. The problem is to determine how much energy each directional wave bin has contributed to the response spectrum of a certain motion as the response spectrum is a summation of energy received from multiple directions. This should be contrasted with model tests. In model tests, RAOs are determined based on uni-directional waves with no wave spreading. The waves can either be regular, random or transient [12, 13], but as long as they are uni-directional, incoming wave direction and resulting vessel motion

can be directly related and the RAOs can be determined based on the quotient of the response and wave spectra [14].

The above mentioned problem has resulted in the question whether, based on measured wave spectra and vessel motions, a method can be developed to calibrate existing RAOs for a change of mass distribution or to obtain a better estimate of viscous damping and potential mass, damping and wave forces. In this paper, a method for calibration is proposed, based on vector fitting [15] of the original RAOs and subsequently modifying the fitting parameters.

The method is tested on an imaginary semi-submersible vessel for 2 test cases. The procedure that has been used is as follows. Based on the results of a diffraction calculation, a set of *standard RAO*s have been determined for the imaginary vessel. Subsequently, for the first test case, mass distribution and viscous roll damping have been changed and *target RAOs* have been determined in the normal manner. For the second test case, the vessel draught has been changed, a new diffraction calculation performed and *target RAOs* have been determined in the normal manner. With the *target RAOs* motion responses have been generated using directional wave spectra that have been encountered during offshore installation projects. For the purpose of this paper, these motion responses represent the 'measured' motions of the imaginary vessel. Then, starting from the motion responses and the original set of *standard RAOs*, it has been attempted to *back-calculate* the *target RAOs*, after which the *target RAOs* and *back-calculated RAOs* are compared.

The imaginary semi-submersible vessel used in the test cases is depicted in Figure 1. The meshing as used in the diffraction calculations is shown as well in this figure. The vessel is symmetrical with respect to the centreline. The origin of the local axis-system used is at [stern, centreline, keel]. With the x-axis positive towards bow, the y-axis positive towards portside and z-axis positive upwards. The vessel has a floater length of 120.0 m and an overall length of 137.5 m. The width of the vessel is 88.0 m. The height of the floaters is 12.0 m and the deck level is at 42.0 m measured from the keel. At 25.0 m draught, the vessel's displacement is 117800 m^3 and the waterplane area is 3570 m^2. The radii of gyration are r_{xx} = 38.7 m, r_{yy} = 52.1 m and r_{zz} = 52.1 m. The position of the CoG is [62.2, 0.0, 24.5] m from [stern, centreline, keel]. The natural period for heave, roll and pitch are 23.8 s, 23.1 s and 17.3 s, respectively.

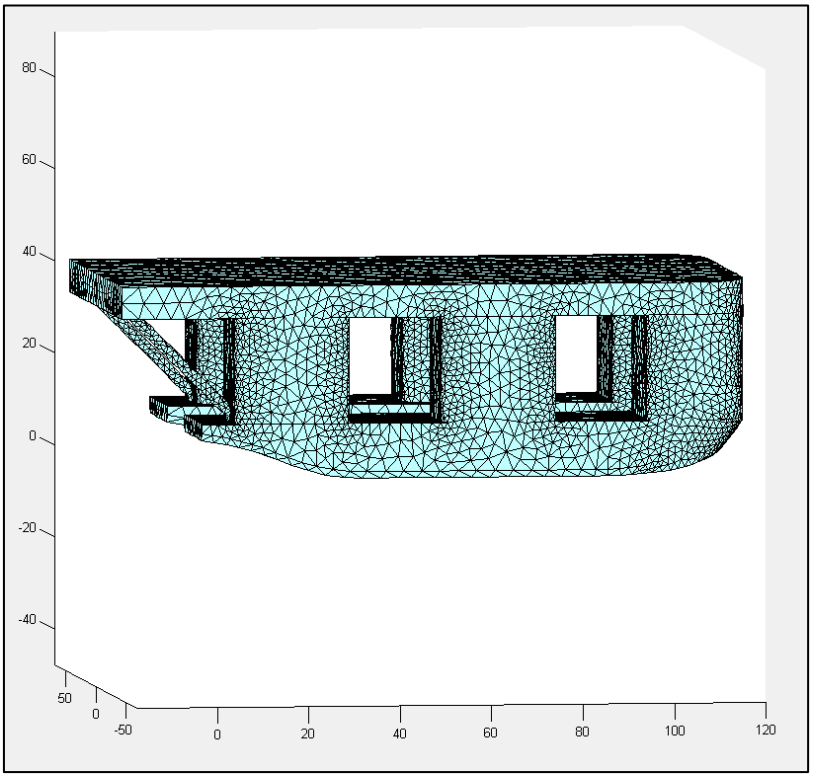

Figure 1: Semi-submersible vessel used in test cases

The vector fitting of the *standard RAOs* is described in Section 3. A novelty here is that the vector fitting method allows for the potential wave forces at intermediate directions to be obtained by interpolation. By relating the variables of the fitting functions to physical quantities and taking the above-discussed causes of RAO inaccuracies into account, an optimization strategy for finding the *target RAOs* is developed in Section 4. Finally, in Section 5, the procedure is applied to the imaginary semi-submersible vessel and the test cases are considered. Conclusions are given in Section 6.

2 CALCULATION OF RAOS

The motion RAOs for the six degrees of freedom (surge, sway, heave, roll, pitch and yaw) are expressed by the following matrix equation [3, 5, 16]:

$$\boldsymbol{RAO}(\omega, dir) = \{-\omega^2 \cdot (\boldsymbol{M} + \boldsymbol{A}(\omega)) + i\omega \cdot (\boldsymbol{B}(\omega) + \boldsymbol{B_{visc}}) + \boldsymbol{C}\}^{-1} \cdot \boldsymbol{F}(\omega, dir) \quad (1)$$

in which $\boldsymbol{M}$ is the mass matrix of the vessel, given by Equation 2 below, $\boldsymbol{A}(\omega)$ is the potential hydrodynamic mass matrix, $\boldsymbol{B}(\omega)$ is the potential hydrodynamic damping matrix, $\boldsymbol{B_{visc}}$ is the damping matrix due to viscous effects, $\boldsymbol{C}$ is the vessel stiffness matrix, given by Equation 3, $\boldsymbol{F}(\omega,dir)$ is the potential hydrodynamic force vector and $\boldsymbol{RAO}(\omega,dir) \in \mathbb{C}^{6x1}$ is the RAO matrix of the vessel for the wave frequency ω and the wave direction *dir*. The hydrodynamic wave forces are calculated for a unit wave with amplitude ζ. The amplitude of the RAOs $\boldsymbol{RAO_a}(\omega, dir)$ represents the motion amplitude per unit wave amplitude, while the phase of the RAOs denotes the phase difference between the vessel motions and the waves. The mass matrix $\boldsymbol{M}$ and stiffness matrix $\boldsymbol{C}$ are defined by:

$$\boldsymbol{M} = \begin{bmatrix} \rho\nabla & 0 & 0 & 0 & 0 & 0 \\ 0 & \rho\nabla & 0 & 0 & 0 & 0 \\ 0 & 0 & \rho\nabla & 0 & 0 & 0 \\ 0 & 0 & 0 & r_{xx}^2\rho\nabla & 0 & 0 \\ 0 & 0 & 0 & 0 & r_{yy}^2\rho\nabla & 0 \\ 0 & 0 & 0 & 0 & 0 & r_{zz}^2\rho\nabla \end{bmatrix} \quad (2)$$

$$\boldsymbol{C} = \begin{bmatrix} 0 & 0 & 0 & 0 & 0 & 0 \\ 0 & 0 & 0 & 0 & 0 & 0 \\ 0 & 0 & \rho g A_{WL} & 0 & -\rho g A_{WL}(x_{CoF} - x_{CoB}) & 0 \\ 0 & 0 & 0 & \rho g \nabla GM_T & 0 & 0 \\ 0 & 0 & -\rho g A_{WL}(x_{CoF} - x_{CoB}) & 0 & \rho g \nabla GM_L & 0 \\ 0 & 0 & 0 & 0 & 0 & 0 \end{bmatrix} \quad (3)$$

In the above equations, ρ denotes the water density, g denotes the acceleration due to gravity, ∇ denotes the vessel displacement, r_{xx}, r_{yy} and r_{zz} are the radii of gyration around the longitudinal, transversal and vertical axes, A_{WL} denotes the vessel's waterplane area, x_{CoF} and x_{CoB} denote the longitudinal coordinates of the vessel's centre of floatation and buoyancy and GM_T and GM_L are the transversal and longitudinal metacentric heights. For small angles of heel or trim, they are given by: $GM_T = KB + BM_T - KG$ and $GM_L = KB + BM_L - KG$, in which KB and KG denote the height of the CoB and CoG above the keel and BM_T and BM_L denote the height of the transverse and longitudinal metacentre above the CoB.

For determination of RAOs, it is normal practice to add diagonal stiffness terms for surge, sway and yaw, such that the resulting natural periods for these motions are very long and fall well outside the wave spectrum.

In this paper RAOs will be determined for the motions of the CoG of the vessel. If the CoG is shifted by a distance [*dx*, *dy*, *dz*], the motions and forces at the shifted CoG can be calculated with linearised transformation matrices [5, 9].

When the RAOs have been determined, the motion response spectra are obtained through integration over the wave directions [3, 5]:

$$\boldsymbol{S_i}(\boldsymbol{\omega}) = \int_{-\boldsymbol{\pi}}^{\boldsymbol{\pi}} \boldsymbol{S_\zeta}(\boldsymbol{\omega}, \boldsymbol{dir}) \cdot \boldsymbol{RAO_{a;i}}(\boldsymbol{\omega}, \boldsymbol{dir})^2 \, \boldsymbol{d(dir)} \quad (4)$$

where i indicates the degree of freedom, S_i is the response spectrum and S_ζ is the wave spectrum.

3 VECTOR FITTING OF THE STANDARD RAOS

The aim of this paper is to back-calculate RAOs based on given motion responses and a set of given *standard RAOs*. Depending on the frequency and wave direction sampling, the matrix containing the standard RAOs can contain a large number of elements. Instead of trying to adjust each element separately, it will be tried to reduce the number of elements to be calibrated by using the method of *vector fitting*.

The method of vector fitting as developed by Semlyen and Gustavsen [15] allows for expressing the frequency-dependent hydrodynamic properties of the vessel (characterized by multiple resonant peaks) in terms of only a limited number of parameters. Similar approaches of approximating the frequency-dependent hydrodynamic properties with complex functions are applied by Liu *et al*. [17, 18] for the determination of frequency response and retardation functions.

An approximation function can be found by fitting a ratio of two polynomials to given frequency-dependent data:

$$f(s) = \frac{a_0 + a_1 s + a_2 s^2 + \cdots + a_N s^N}{b_0 + b_1 s + b_2 s^2 + \cdots + b_N s^N} \tag{5}$$

where $s = i\omega$ and $f(s)$ represents the frequency dependent data. In order to find the unknown coefficients of the polynomial, Equation 9 is written as a linear matrix equation of the type $\boldsymbol{Ax} = \boldsymbol{b}$. This can be achieved by multiplying both sides with the denominator. The resulting problem is, however, badly scaled, as the columns of $\boldsymbol{A}$ are multiplied by different powers of s. Only low-order approximations can thus be found using this relation. To avoid this limitation, the data are approximated by fitting partial fractions with pre-calculated resonant complex poles [15]. The equation for the approximation function then becomes:

$$f(s) = \sum_{n=1}^{N} \left(\frac{\mathrm{c}_n}{s - p_n} \right) + d + s \cdot h \tag{6}$$

where c_n are the complex residues, p_n are the complex resonant poles, d and h are real quantities and N is the total amount of resonant poles. Both the residues and the poles come in complex conjugate pairs.

Each parameter plays a certain role in defining the characteristics of the resulting approximation function. By selecting the appropriate values of these parameters, a curve with resonant peaks of a specific amplitude and shape can be created. It is useful to mention the following:

- The frequencies at which the approximation curve displays resonant peaks are specified by the imaginary part of the poles.
- The amplitudes of the real parts of the poles specify the sharpness of the resonant peaks.
- The moduli of the residues specify the amplitude of the resonant peaks.
- The parameter d lifts the curve of the approximation function.
- The parameter h tilts the curve of the approximation function.

The vector fitting procedure as developed by Semlyen and Gustavsen, consists of two stages. In the first stage, a set of complex poles distributed over the frequency range of interest is selected. In the second stage the remaining parameters are determined based on the poles as identified in stage 1.

It should be noted that the selection of the initial poles has an important effect on the accuracy of the approximation. A practical location of the initial poles should thus be decided on. These poles are complex conjugate pairs distributed over the frequency range, and can be written as follows:

$$p_n = -\alpha_{pn} + i\beta_{pn} \;\; , \;\; p_{n+1} = -\alpha_{pn} - i\beta_{pn} \tag{7}$$

where p_n, p_{n+1} is a conjugate pair of complex poles, and α_{pn}, β_{pn} are the real and imaginary parts of the pole, respectively. It is assumed that the real parts of the initial poles are given by: $\alpha_{pn} = \frac{\beta_{pn}}{100}$ [15].

In what follows, the vector fitting for a) the added mass and damping and b) the wave forces, will be discussed separately. The process is applied to the added mass, damping and wave forces of the imaginary semi-submersible vessel described in Section 1.

3.1 Vector fitting of the added mass and damping

The vector fitting method is applied to approximate the frequency domain elements of the added mass and damping matrices. Based on potential theory, added mass and damping are mathematically related through the Kramers-Kronig relations, and should thus not be treated separately [19]. The fitting process is accomplished for the complex number *ab* which is related to the added mass *a* and damping *b* in the following manner:

$$ab_{ij}(\omega) = a_{ij}(\omega) - \frac{b_{ij}(\omega)}{\omega} \cdot i \tag{8}$$

where a_{ij} is an element of the added mass matrix, b_{ij} an element of the damping matrix, and ω the wave frequency. In total, the added mass and damping matrices have 36 frequency-dependent elements of which 18 are zero. A maximum of 18 approximation functions should thus be constructed.

Furthermore, when considering the vessel having a vertical-longitudinal plane of symmetry the motions can be split into symmetric and anti-symmetric components, further reducing the number of unknowns. Surge, heave and pitch are coupled symmetric motions, while sway, roll and yaw then become coupled anti-symmetric motions. Taking advantage of symmetry and anti-symmetry conditions, the number of approximation functions can be reduced from 18 to 12.

Each of these elements of the hydrodynamic added mass and damping matrices is replaced by a fitting function as shown below:

$$\mathbf{A}(\omega)= \begin{bmatrix} a_{11}(\omega) & 0 & a_{13}(\omega) & 0 & a_{15}(\omega) & 0 \\ 0 & a_{22}(\omega) & 0 & a_{24}(\omega) & 0 & a_{26}(\omega) \\ a_{31}(\omega) & 0 & a_{33}(\omega) & 0 & a_{35}(\omega) & 0 \\ 0 & a_{42}(\omega) & 0 & a_{44}(\omega) & 0 & a_{46}(\omega) \\ a_{51}(\omega) & 0 & a_{53}(\omega) & 0 & a_{55}(\omega) & 0 \\ 0 & a_{62}(\omega) & 0 & a_{64}(\omega) & 0 & a_{66}(\omega) \end{bmatrix} \rightarrow \begin{bmatrix} \Re\{f_{ab_{11}}(s)\} & 0 & \Re\{f_{ab_{13}}(s)\} & 0 & \Re\{f_{ab_{15}}(s)\} & 0 \\ 0 & \Re\{f_{ab_{22}}(s)\} & 0 & \Re\{f_{ab_{24}}(s)\} & 0 & \Re\{f_{ab_{26}}(s)\} \\ \Re\{f_{ab_{31}}(s)\} & 0 & \Re\{f_{ab_{33}}(s)\} & 0 & \Re\{f_{ab_{35}}(s)\} & 0 \\ 0 & \Re\{f_{ab_{42}}(s)\} & 0 & \Re\{f_{ab_{44}}(s)\} & 0 & \Re\{f_{ab_{46}}(s)\} \\ \Re\{f_{ab_{51}}(s)\} & 0 & \Re\{f_{ab_{53}}(s)\} & 0 & \Re\{f_{ab_{55}}(s)\} & 0 \\ 0 & \Re\{f_{ab_{62}}(s)\} & 0 & \Re\{f_{ab_{64}}(s)\} & 0 & \Re\{f_{ab_{66}}(s)\} \end{bmatrix}$$

(9)

$$\mathbf{B}(\omega)= \begin{bmatrix} b_{11}(\omega) & 0 & b_{13}(\omega) & 0 & b_{15}(\omega) & 0 \\ 0 & b_{22}(\omega) & 0 & b_{24}(\omega) & 0 & b_{26}(\omega) \\ b_{31}(\omega) & 0 & b_{33}(\omega) & 0 & b_{35}(\omega) & 0 \\ 0 & b_{42}(\omega) & 0 & b_{44}(\omega) & 0 & b_{46}(\omega) \\ b_{51}(\omega) & 0 & b_{53}(\omega) & 0 & b_{55}(\omega) & 0 \\ 0 & b_{62}(\omega) & 0 & b_{64}(\omega) & 0 & b_{66}(\omega) \end{bmatrix} \rightarrow \begin{bmatrix} \Im\{f_{ab_{11}}(s)\} & 0 & \Im\{f_{ab_{13}}(s)\} & 0 & \Im\{f_{ab_{15}}(s)\} & 0 \\ 0 & \Im\{f_{ab_{22}}(s)\} & 0 & \Im\{f_{ab_{24}}(s)\} & 0 & \Im\{f_{ab_{26}}(s)\} \\ \Im\{f_{ab_{31}}(s)\} & 0 & \Im\{f_{ab_{33}}(s)\} & 0 & \Im\{f_{ab_{35}}(s)\} & 0 \\ 0 & \Im\{f_{ab_{42}}(s)\} & 0 & \Im\{f_{ab_{44}}(s)\} & 0 & \Im\{f_{ab_{46}}(s)\} \\ \Im\{f_{ab_{51}}(s)\} & 0 & \Im\{f_{ab_{53}}(s)\} & 0 & \Im\{f_{ab_{55}}(s)\} & 0 \\ 0 & \Im\{f_{ab_{62}}(s)\} & 0 & \Im\{f_{ab_{64}}(s)\} & 0 & \Im\{f_{ab_{66}}(s)\} \end{bmatrix}$$

(10)

where, according to Equation 10:

$f_{ab11}(s) = \sum_{n=1}^{N} \frac{c_{n,ab11}}{s - p_{n,ab11}} + d_{ab11} + s \cdot h_{ab11}$ and so forth.

For the selection of the initial poles in stage 1 of the vector fitting, it is suggested to use the local minima and maxima of the amplitudes of ab_{ij}. In accordance with the explanation given above, the wave frequencies that correspond to these minima and maxima are used as the

imaginary part of the initial poles. The real parts of the initial poles are then calculated by dividing the imaginary part by 100 [15]. Due to the fact that the vessel motions are mainly influenced by wind-sea and swell, the curve fitting has been performed for the frequency range of 0.15-1.60 rad/s, thus avoiding the selection of poles at frequencies outside this range. Furthermore, several iterations should be performed to get a better set of poles. The iterations stop when the scaling function reaches a minimum value [15]. In the second stage of the vector fitting process, the residues and the real quantities of the final approximation function have been identified.

To evaluate the accuracy of the fitting process, the Normalized Root Mean Square Error [20] is used:

$$NRMSE_{abij} = 1 - \frac{\sqrt{\frac{1}{k}\cdot\sum_{i=1}^{k}\left(ab_{ij,VF}(\omega_i) - ab_{ij,OR}(\omega_i)\right)^2}}{\sqrt{\frac{1}{k}\cdot\sum_{i=1}^{k}\left(ab_{ij,OR}(\omega_i) - mean(ab_{ij,OR})\right)^2}} \tag{11}$$

where $ab_{ij,VF}$ and $ab_{ij,OR}$ represent the approximated and original values of element ab_{ij}, respectively, and k is the total number of wave frequencies. The denominator corresponds to the standard deviation of the original values of element ab_{ij}.

The NRMSE varies from $-\infty$ (bad fit) to 1 (perfect fit). The NRMSEs obtained for fitting of the potential mass and damping of the imaginary vessel considered in this paper are shown in Table 1, where it can be seen that the fitting functions approximate the data with accuracy. Figure 2 and Figure 3 below show the fitted and original curves for the elements a_{33} and b_{33} (the best fit), and a_{64} and b_{64} (the worst fit), respectively.

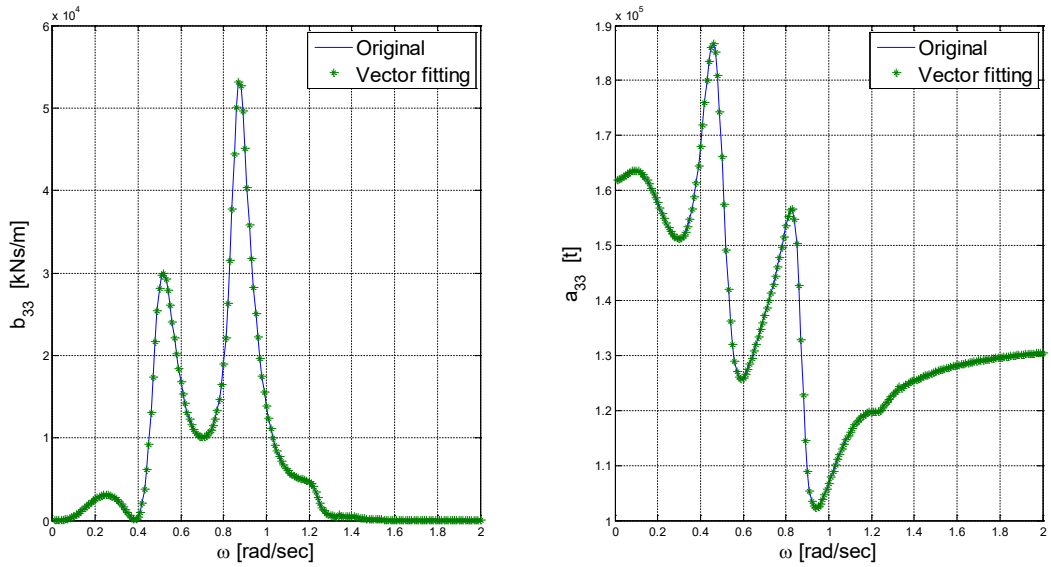

Figure 2: Vector fitting for hydrodynamic damping b_{33} and added mass a_{33}

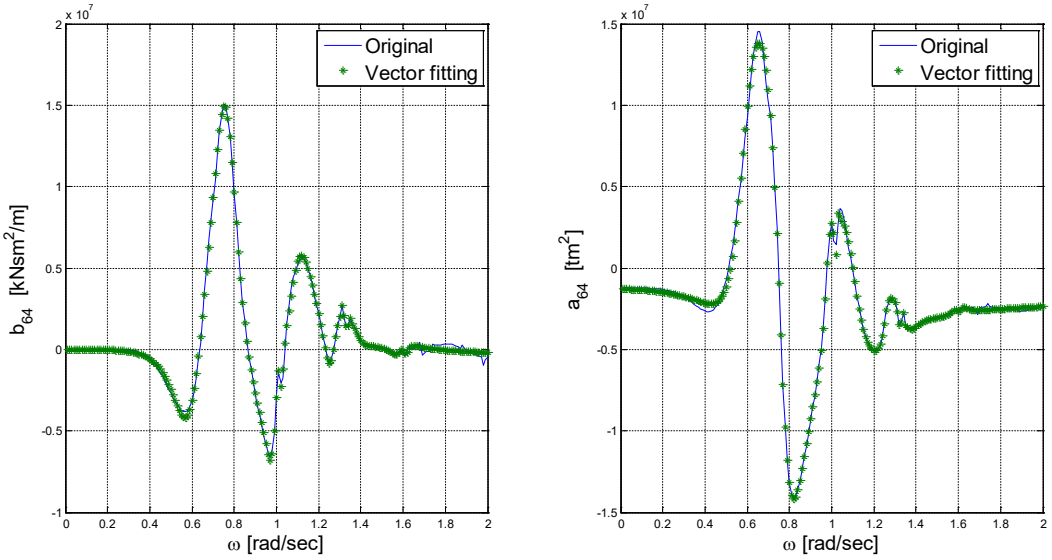

Figure 3: Vector fitting for hydrodynamic damping b_{64} and added mass a_{64}

Table 1: Normalized Root Mean Square Error: Potential added mass and damping

ab_{11}	ab_{22}	ab_{31}	ab_{33}	ab_{42}	ab_{44}	ab_{51}	ab_{53}	ab_{55}	ab_{62}	ab_{64}	ab_{66}
0.990	0.976	0.987	0.998	0.996	0.998	0.990	0.993	0.984	0.968	0.951	0.982

The number of poles used for each element of the potential added mass and damping is shown in the following table:

Table 2: Number of poles used for the vector fitting of potential added mass and damping

ab_{11}	ab_{22}	ab_{31}	ab_{33}	ab_{42}	ab_{44}	ab_{51}	ab_{53}	ab_{55}	ab_{62}	ab_{64}	ab_{66}
20	22	22	22	28	12	22	18	16	26	22	24

3.2 Vector fitting of the wave forces

Diffraction software suites typically provide frequency-dependent hydrodynamic forces for 6 DoFs and 24 wave directions. For every wave direction, there is a set of 6 hydrodynamic forces, corresponding to the 6 vessel motions. In this paper, the wave directions are considered in steps of 15 degrees. As a result, a maximum of 144 approximation functions should be found for the wave forces.

This number of fitting functions can, however, again be reduced based on symmetry and anti-symmetry conditions. The forces that are related to symmetric motions have the same amplitude and phase for symmetric angles of wave heading with respect to the longitudinal axis of the vessel. Additionally, the forces that are related to anti-symmetric motions have the same amplitude, but opposite phases, for those wave headings. Considering this, only approximation functions corresponding to the range 0 to 180 degrees of wave headings have to be found.

For example, the matrix for the wave forces of 0^o wave heading is defined below:

$$\boldsymbol{F}(\omega,0^\circ)=\begin{bmatrix} F_1(\omega_1,0^\circ) & \cdots & F_1(\omega_k,0^\circ) \\ \vdots & \ddots & \vdots \\ F_6(\omega_1,0^\circ) & \cdots & F_6(\omega_k,0^\circ) \end{bmatrix} \tag{12}$$

where k is again the number of wave frequencies.

After applying the fitting functions, the matrix becomes:

$$\boldsymbol{F}(\omega,0^\circ)=\begin{bmatrix} f_1(s_1,0^\circ)\ldots f_1(s_k,0^\circ) \\ f_2(s_1,0^\circ)\ldots f_2(s_k,0^\circ) \\ \vdots \\ f_6(s_1,0^\circ)\ldots f_6(s_k,0^\circ) \end{bmatrix}, \text{ where: } f_1(s,0^\circ)=\sum_{n=1}^{N}\frac{c_{n,F_1\_0^\circ}}{s-\mathrm{p}_{n,F_1\_0^\circ}}, \text{etc} \tag{13}$$

The same fitting functions are used for symmetric wave headings:

$$f_1(s,345^\circ)=\ f_1(s,15^\circ),\quad f_3(s,345^\circ)=\ f_3(s,15^\circ),\quad f_5(s,345^\circ)=\ f_5(s,15^\circ)$$
$$f_2(s,345^\circ)=-f_2(s,15^\circ),\quad f_4(s,345^\circ)=-f_4(s,15^\circ),\quad f_6(s,345^\circ)=-f_6(s,15^\circ) \tag{14}$$

In addition, it is noticed that the real quantities d and h can be omitted from the fitting functions.

For each of the 6 wave forces, it is suggested to use the same poles for the entire range of 0 to 180 degrees of wave headings. First, a set of poles is identified for the force that corresponds to the wave direction with the highest number of peaks. This set of poles is then applied for the approximation functions for all the wave directions. For the directions with less resonant peaks, the residues related to the extra poles will be assigned low values. The remainder of the process for the vector fitting of the wave force in the direction containing the maximum number of resonant peaks is the same as described in the previous section. Given the fitted poles in this direction, only the second stage of vector fitting is accomplished for the rest of the wave directions (identification of residues).

The NRMSEs obtained for the fitting of the wave forces are shown in Table 3. It can be seen that the fitting functions are less accurate than for the fitting of the potential mass and damping. The best and worst fit are depicted in Figure 4 and Figure 5. It is, however, expected that the fitting is still good enough for the purpose of this paper. This assumption will be checked in the next section.

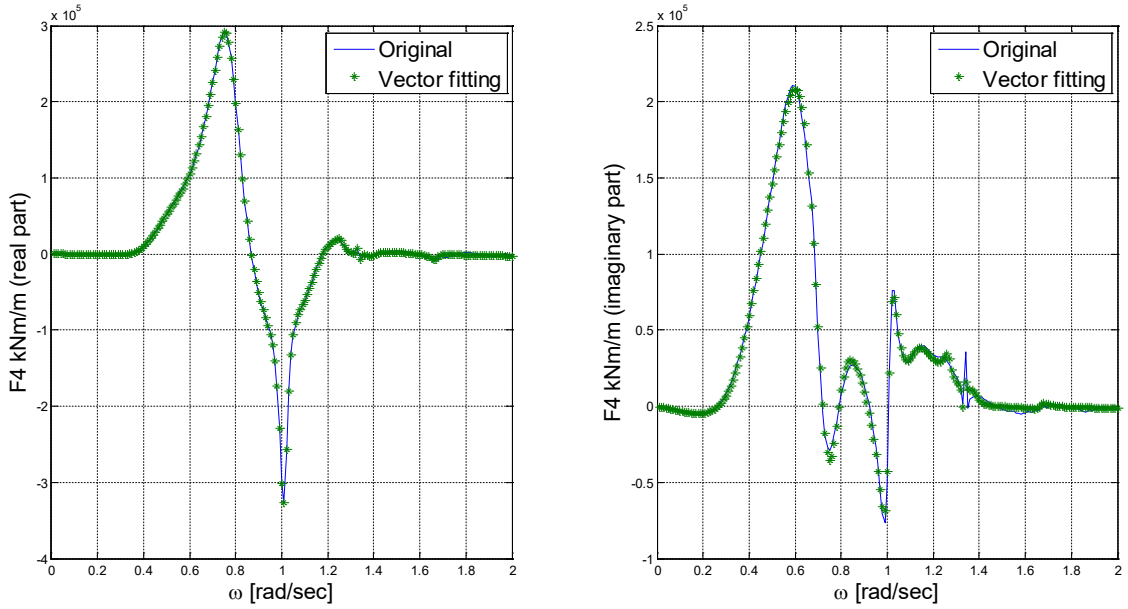

Figure 4: Real and imaginary parts of F_4, direction = 75°

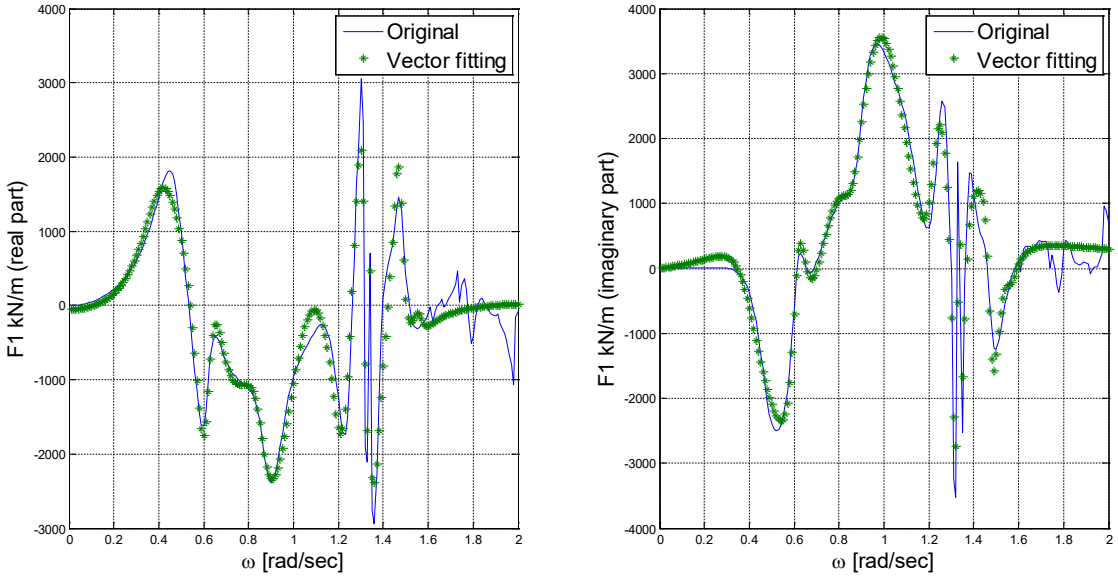

Figure 5: Real and imaginary parts of F_1, direction = 90º

Table 3: Normalized Root Mean Square Error: Wave forces

NRMSE	F1	F1	F3	F4	F5	F6
0º	0.911	-	0.836	-	0.956	-
15º	0.928	0.898	0.863	0.827	0.961	0.856
30º	0.932	0.942	0.877	0.867	0.974	0.874
45º	0.952	0.965	0.918	0.920	0.958	0.791
60º	0.838	0.946	0.949	0.949	0.939	0.778
75º	0.891	0.946	0.968	0.992	0.938	0.875
90º	0.766	0.934	0.969	0.956	0.945	0.859
105º	0.880	0.955	0.954	0.953	0.933	0.876
120º	0.912	0.945	0.927	0.961	0.928	0.882
135º	0.906	0.941	0.859	0.969	0.917	0.904
150º	0.903	0.907	0.853	0.951	0.929	0.921
165º	0.920	0.902	0.885	0.953	0.956	0.978
180º	0.909	-	0.891	-	0.933	-

The number of poles used for each of the wave forces is shown in the following table:

Table 4: Number of poles used for the vector fitting of the wave forces

F1	F1	F3	F4	F5	F6
30	42	20	26	32	32

The vector fitting method provides a suitable means to express the hydrodynamic properties of the vessel using only a limited number of parameters. Furthermore, the implementation of the same poles for all wave directions is an advantage for the interpolation of the wave forces over the wave directions. Only by interpolating the residues, the wave forces for the in-between wave directions can be determined.

3.3 Fitted standard RAOs and motion spectra

Having obtained approximation functions for the potential added mass, damping and wave forces, the RAOs can be calculated according to Equation 1. These RAOs are now compared to those obtained using the original vessel matrices. The NRMSEs calculated for the frequency range of 0.20-1.60 rad/s are shown in Table 5. The best and worst fits are again shown in Figure 6 and Figure 7, respectively.

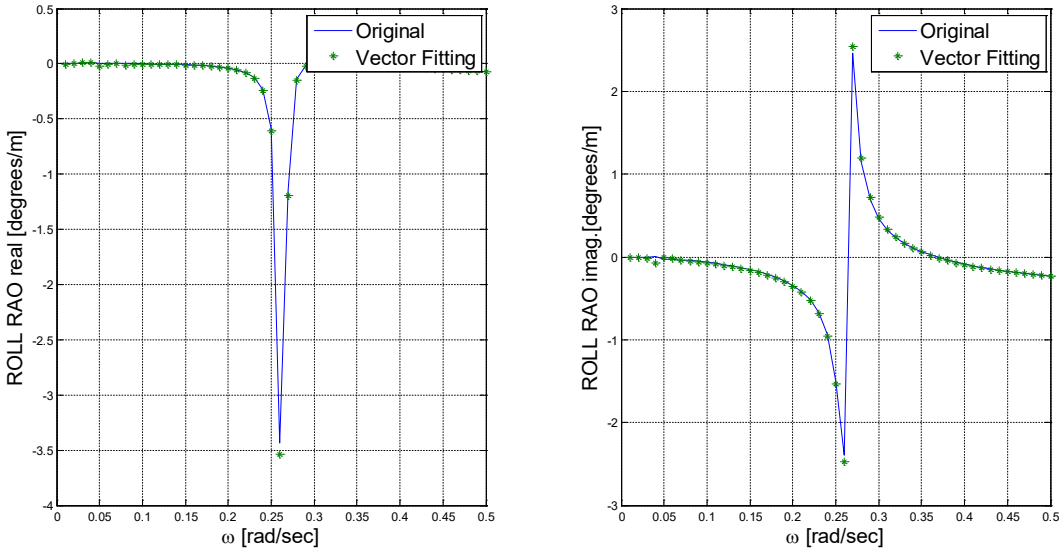

Figure 6: Roll RAO, 75 degrees, real and imaginary parts

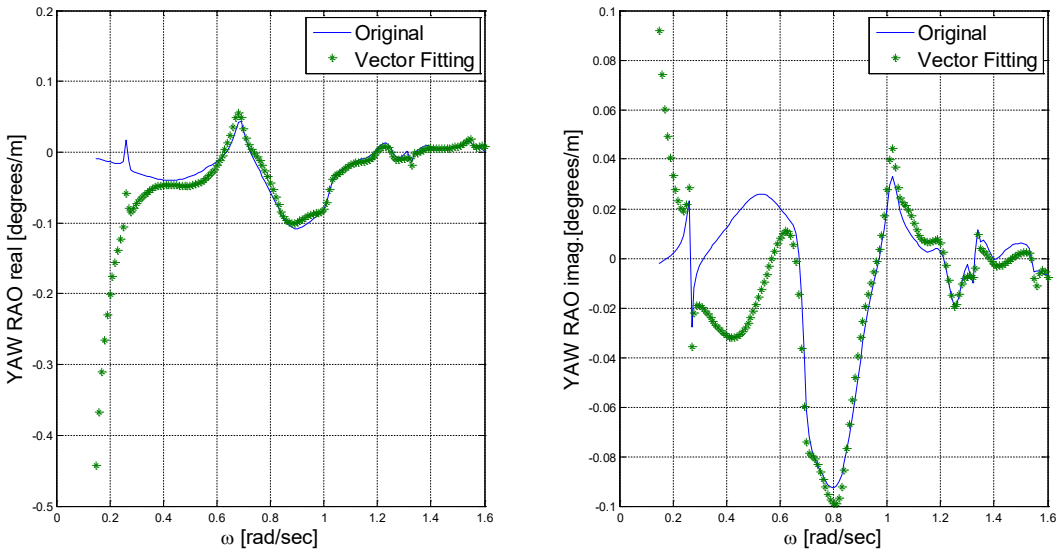

Figure 7: Yaw RAO, 60 degrees, real and imaginary parts

Table 5: Normalized Root Mean Square Error: RAOs

Wave dir.\Motion	SURGE	SWAY	HEAVE	ROLL	PITCH	YAW
0º	0.914	-	0.912	-	0.922	-
15º	0.909	0.902	0.914	0.240	0.927	0.642
30º	0.910	0.912	0.926	0.472	0.931	0.808
45º	0.912	0.912	0.961	0.723	0.947	0.249
60º	0.899	0.924	0.935	0.845	0.947	0.134
75º	0.920	0.917	0.954	0.968	0.894	0.496
90º	0.756	0.921	0.965	0.939	0.801	0.176
105º	0.920	0.922	0.964	0.883	0.791	0.740
120º	0.934	0.925	0.933	0.941	0.835	0.696
135º	0.929	0.922	0.840	0.898	0.840	0.767
150º	0.926	0.924	0.811	0.803	0.868	0.833
165º	0.921	0.906	0.826	0.911	0.877	0.967
180º	0.927	-	0.828	-	0.876	-

In the last part of this section, the motion responses of the vessel as calculated by the *standard RAOs* and the *fitted standard RAOs* are compared. As wave input, a directional spectrum as encountered during an offshore installation project, has been used. The significant wave height of the spectrum is H_s = 1.4 m. The spectrum is presented in Figure 8. The vessel is experiencing wind seas coming from the Northnortheast and the East.

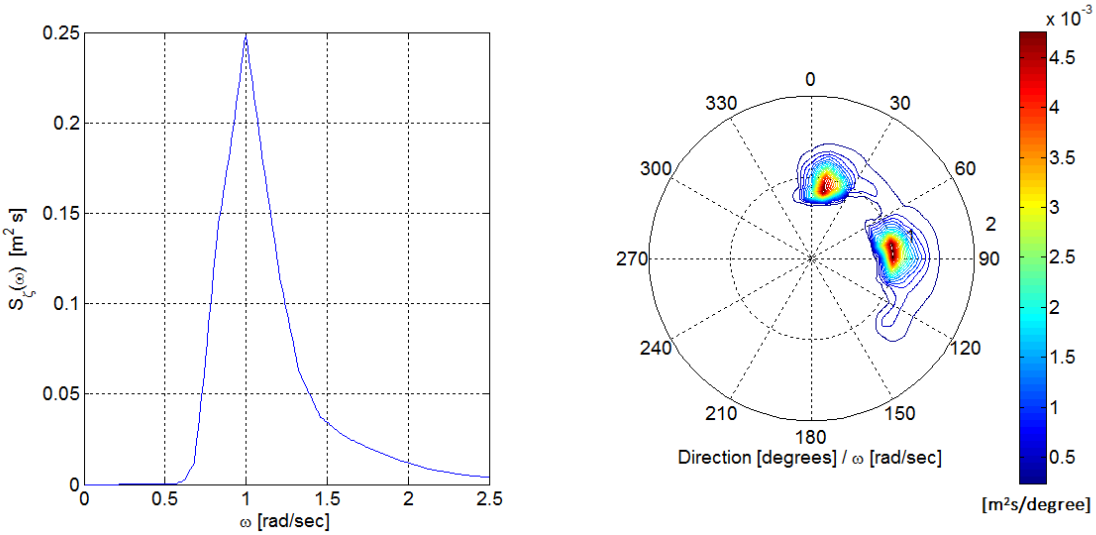

Figure 8: Wave spectrum used for motion comparison

The heading of the vessel is assumed to be 45° (Northeast). The responses obtained using the *fitted* and original *standard RAOs* are compared in Figure 9:

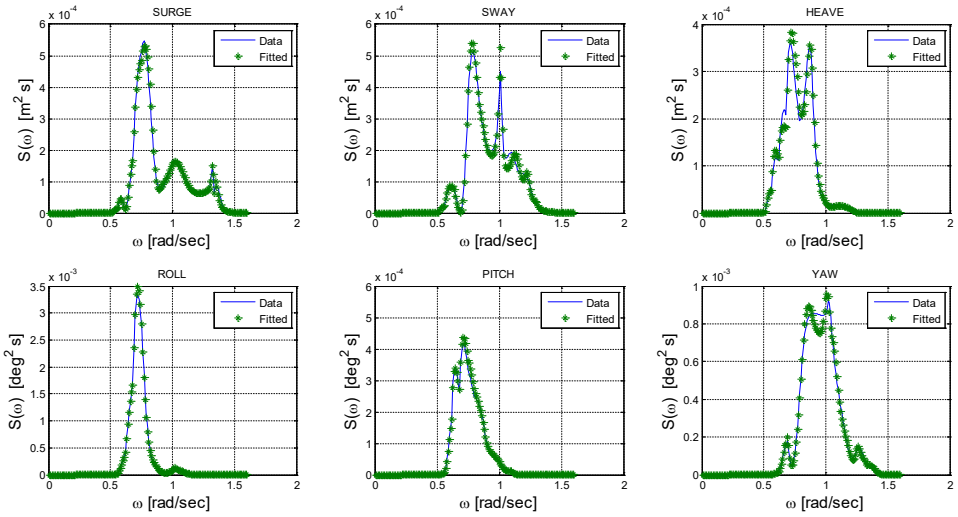

Figure 9: Motion response spectra using fitted and original standard RAO

To analyze the fit, the significant values of the fitted and original response spectra for the 6 vessel motions are calculated as follows:

$$X_{s,i} = 4 \cdot \sqrt{\int_0^\infty S_i(\omega) \cdot d\omega} \tag{15}$$

where i indicates the vessel DoF.

These significant values are compared in the following table:

Table 6: Significant responses calculated with *Fitted* and *Original* standard RAOs

Motions \ Significant value	Fitted	Original	Error
SURGE (cm)	4.59	4.61	-0.02
SWAY (cm)	4.82	4.84	-0.02
HEAVE (cm)	3.84	3.90	-0.07
ROLL (degrees*10^{-2})	8.15	8.18	-0.03
PITCH (degrees*10^{-2})	3.86	3.92	-0.05
YAW (degrees*10^{-2})	6.99	6.97	0.02

The inaccuracies in the fitted standard RAOs do not influence the final response spectra. The large errors obtained in the low-frequency ranges for certain RAOs (see Figure 7) do not effect the final motion response, since the wave energy in these frequency ranges is insignificant.

4 CALIBRATION OF FITTED RAOS

After application of the vector fitting method, the *fitted standard RAOs* for the vessel motions have become a function of the fitting parameters for the potential mass, damping and wave forces and of the orginal mass matrix $\boldsymbol{M}$, damping matrix $\boldsymbol{B}_{visc}$ and stiffness matrix $\boldsymbol{C}$, which themselves are functions of displacement, radii of gyration, waterplane area, metacenter heights and CoG position. The aim is to calibrate these quantities based only on given wave and response spectra. In this paper, the focus will lie on calibration of the CoG position, the radii of gyration, the viscous roll damping and the fitting parameters for the potential mass, damping and wave forces, for the reasons discussed in Section 1. Five algorithms have been created, corresponding to the calibration of the CoG, the radii of gyration, the viscous damping, the hydrodynamic added mass-damping, and the hydrodynamic forces, respectively. These algorithms are based on the following steps:

1. The vessel motions are calculated based on the original vessel properties with the *fitted standard RAOs*. Then the resulting response spectra are compared with the vessel response spectra of the given data set. This comparison is accomplished by calculating the normalized root mean square error of each vessel motion. Therefore, 6 NRMSEs are obtained in total. Then the average of these 6 values is determined.
2. For the parameter to be calibrated, a wide interval of possible values is defined.
3. By using the 'golden section method', a value within the before mentioned interval is chosen.
4. The motion response spectra are re-calculated based on the new value of the parameter.
5. The new response spectra are compared with the response spectra of the data set in terms of average NRMSEs.
6. By comparing the two averages of the NRMSEs of step 1 and step 5, a smaller interval of values for the parameter can be obtained. More details about the determination of the new interval of values, are provided in Section 4.1.
7. The process is repeated until the interval of values is acceptably small or the NRMSE cannot be further improved.

4.1 Golden section method

The golden section method is applied to minimize the number of iterations required to optimize each parameter. Based on the work of Press, Teukolsky, Vetterling and Flannery [21], the method is illustrated using as example the identification of the radius of gyration r_{yy}. The maximum NRMSE for the roll motion is bracketed by a triplet of values of r_{yy}. The three different values of r_{yy} ($\alpha < \beta < \gamma$) are such that the NRMSE of the response spectrum for $r_{yy} = \beta$ is larger than the NRMSEs for $r_{yy} = \alpha$ and $r_{yy} = \gamma$. Therefore, it is concluded that the NRMSE has a maximum within the interval [α, γ]. The next step is to choose a new point χ, either between α and β or between β and γ. Suppose that the latter choice is made, then the NRMSE for $r_{yy} = \chi$ will be evaluated. If the NRMSE for $r_{yy} = \beta$ is larger than the NRMSE for $r_{yy} = \chi$, then the new bracketing triplet of points is [α, β, χ]. For the opposite case, the new bracketing triplet is [β, χ, γ]. In all cases the middle point of the new triplet is the best maximum achieved so far. For each stage, the point χ has a fractional distance 0.61803 into the larger of the two intervals, [α, β] or [β, γ]. This fractional distance is the so-called golden section or golden mean [21]. It should be clear that the limits of the NRMSE are $-\infty$, for poor approximations, and 1, for perfect approximations. Thus, modifications that lead to NRMSEs close to 1, are searched for.

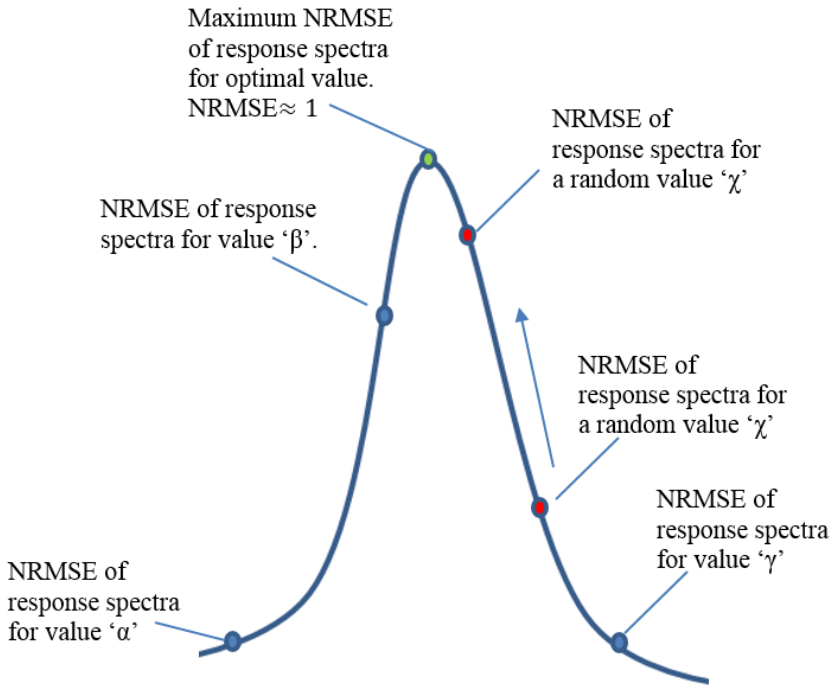

Figure 10: Golden section method [21]

To stop the repetitions of the golden section method, the following conditions should be defined:

1. Minimum distance between the limits of the final bracketing interval.
2. Minimum difference between the resulting NRMSEs of the triplet.

It should be noted that the golden section method is a numerical method to make guesses for the solution to the inverse problem. This can lead to values which do not correspond to the true underlaying physics.

4.2 Algorithms for the calibration of the RAOs

The algorithms for calibration of the CoG position and the radii of gyration are very similar. Each coordinate of the CoG and each radius of gyration is investigated separately. In the case of a symmetrical vessel like a semi-submersible, each radius of gyration mainly influences one specific motion. For instance, to calibrate the yaw motion, the radius of gyration r_{zz} is investigated according to the NRMSE for yaw motion. Regarding the identification of the CoG, each coordinate influences more than one motion and as a consequence the average error of all vessel motions should be considered. The algorithm for calibration of the radii of gyration is depicted in Figure 11.

The viscous damping is most important for the roll motion as the damping of the other motions is governed by the potential damping. Therefore, regarding the matrix of the viscous damping, only the element $B_{visc}(4,4)$ is calibrated. Only large changes to the magnitude of the viscous damping cause considerable changes to the response spectra. As a result, unrealistic values for the viscous damping can be produced by the calibration method. It is therefore suggested to examine the viscous damping matrix at the end of the identification process.

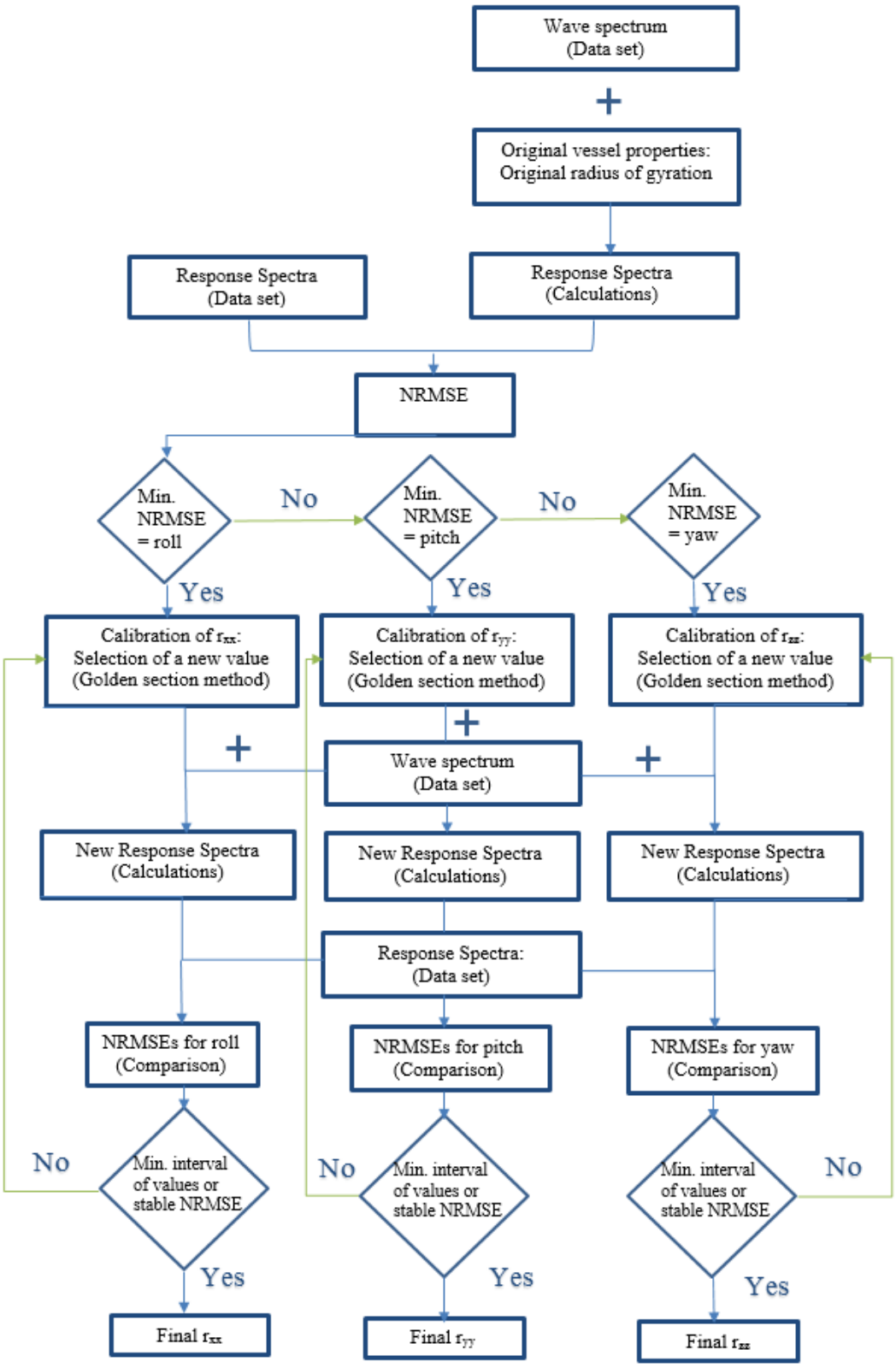

Figure 11: Algorithm for calibration of the radii of gyration

With respect to the identification of the hydrodynamic added mass and damping, the focus lies again on the motions showing the maximum inaccuracies. Because of the symmetry, anti-symmetry conditions of the semi-submersible vessel, the amount of elements that will be investigated can be reduced. For example, if the roll motion indicates the highest error, only the elements with indices 2, 4, 6 are calibrated. The identification procedure of the added mass and damping is similar to the previously described procedures. However, the procedure is performed only for the conjugate pairs of residues. The residues are tested by going over the matrix, element by element. After testing all relevant residues, only the single pair of residues that improves the NRMSE the most, is calibrated.

For the calibration of the wave forces, the algorithm starts with determining the motions with the maximum inaccuracies as well. If the pitch motion indicates the highest error, only F_1, F_3 and F_5 are calibrated. In addition, for pitch, the hydrodynamic forces with directions within the range of -45° to +45° from the main wave direction are investigated. The output of this algorithm gives a modified conjugate pair of residues of a specific force with a certain wave direction.

As described before, each algorithm gives one optimal value for one quantity or parameter. Thus, 5 possible solutions are obtained: a calibrated value for a radius of gyration, for the CoG position, for one element of the viscous damping matrix, for one conjugate pair of residues of one element of the added mass and damping matrices and for one conjugate pair of residues of one wave force of one wave direction. Among these 5 solutions, the parameter which leads to the maximum NRMSE is chosen. After modifying only this parameter, all the algorithms are performed again. In the same way, another parameter is investigated and modified. After several repetitions the NRMSEs reach a certain limit. This means that all the possible parameters are already calibrated and any additional change does not improve the accuracy of the calculated response spectra.

5 TEST CASES

The calibration method for the motion RAOs is tested with 2 cases. The procedure that has been used is as follows. The vessel mass distribution and hydrodynamic properties have been slightly changed. Based on a diffraction calculation, a set of *target RAOs* have been determined in the normal manner. With the *target RAOs* motion responses have been generated using directional wave spectra that have been encountered during offshore installation projects. For the purpose of this paper, these motion responses represent the 'measured' motions of the imaginary vessel. Then, starting from these motion responses and the set of *fitted standard RAOs*, it has been attempted to *back-calculate* the *target RAOs*, after which the *target RAOs* and *back-calculated RAOs* are compared.

For the first test case, mass distribution (r_{yy}, r_{zz}, z_{CoG}) and viscous roll damping have been changed. To examine whether the calibration procedure can be used to improve vessel RAOs when the potential mass and damping matrix and the potential wave forces are inaccurate, in the second test case it will be attempted to adjust the potential mass, damping and wave forces for a change in vessel draught.

5.1 Test case 1

The directional wave spectrum used in Test case 1 is depicted in Figure 12. The significant wave height of the spectrum is H_s = 2.7 m. The vessel is experiencing seas coming from the Eastsoutheast. The heading of the vessel is -30° (approximately Northnorthwest).

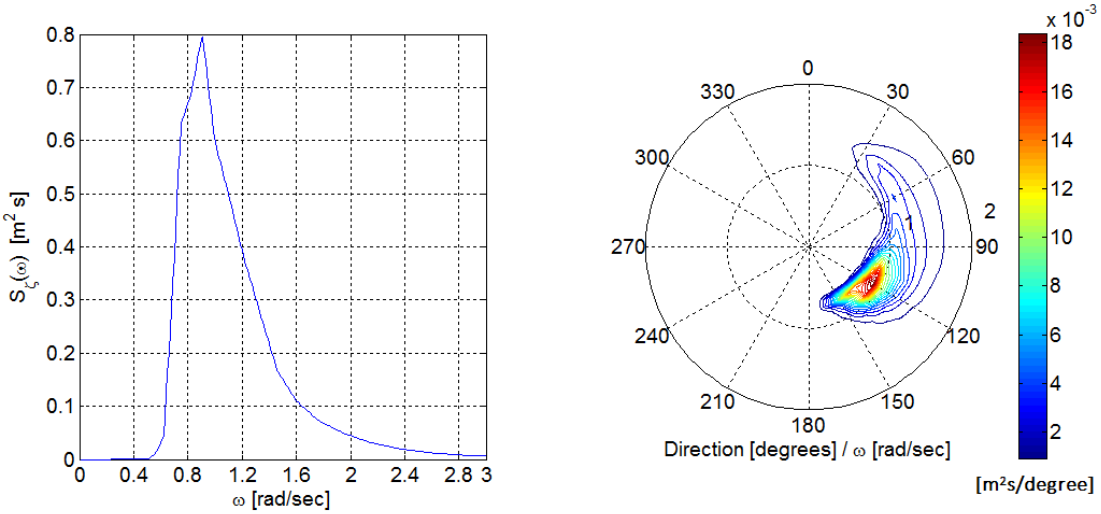

Figure 12: Wave spectrum used in Test case 1

With the *fitted standard RAOs* the vessel responses are calculated. The calculated motion spectra are compared with the spectra of the given data set in Figure 13. The initial NRMSEs for each of the vessel motions are as follows: surge = 0.967, sway = 0.943, heave = 0.985, roll = 0.837, pitch = 0.281, yaw = 0.836.

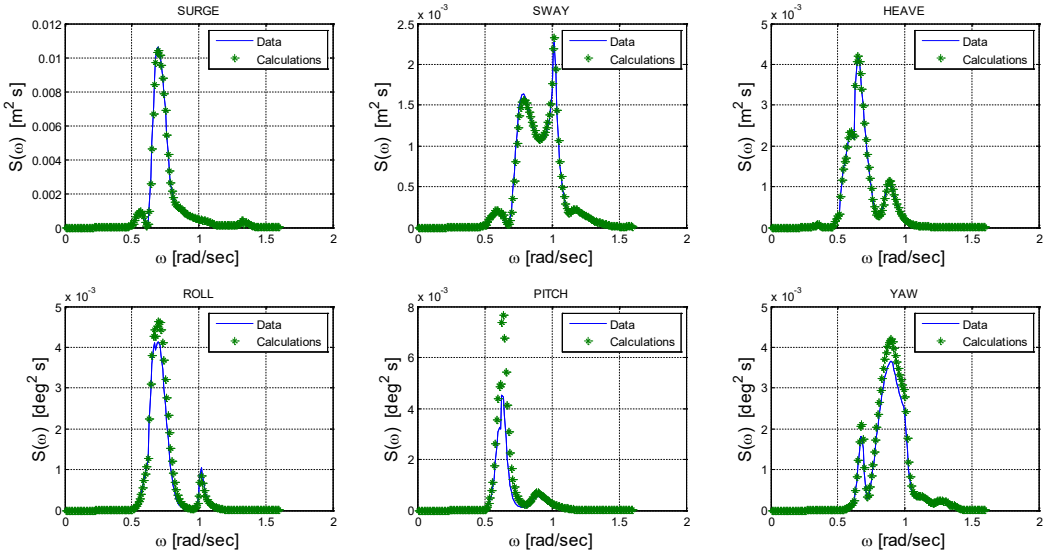

Figure 13: Comparison of *given* response spectra with spectra as calculated with *fitted standard RAOs*, Test case 1

For each repetition the effect of modifying the CoG position, the radii of gyration and the viscous roll damping have been investigated. The results of the calibration procedure for Test case 1 are given in Table 7. To keep the table readable, for each repetition only the modifications of the parameters resulting in the largest possible increase of the NRMSE are shown.

As stated in the previous section, the original value of $B_{visc}(4,4)$ should be changed only in the last repetition of the identification procedure. For each repetition the element that causes the highest accuracy to the response spectra is selected to be modified. In Table 7, the cell of this parameter is shaded grey.

Table 7: Calibration procedure, Test case 1

Parameter	Original Value	Repetition 1	Deviation
z_{CoG} (m)	24.5	30.7	6.2
Average (NRMSEs)	0.808	0.894	0.086
r_{zz} (m)	52.1	54.7	2.6
Yaw motion (NRMSE)	0.836	0.997	0.161
B_{visc}(4,4) (kNsm^2/m)	2.20E+06	3.28E+07	14.9* Orig.value
Roll motion (NRMSE)	0.837	0.904	0.067
Selected Modification:		**r_{zz} = 54.7 m**	
Parameter	**Repetition 1**	**Repetition 2**	**Deviation**
z_{CoG} (m)	*24.5*	*30.1*	*5.6*
Average (NRMSEs)	*0.835*	*0.922*	*0.087*
r_{yy} (m)	*52.1*	*59.6*	*7.5*
Pitch motion (NRMSE)	*0.281*	*0.878*	*0.597*
B_{visc} (4,4) (kNsm^2/m)	2.20E+06	3.14E+07	14.3* Orig.value
Roll motion (NRMSE)	0.837	0.903	0.066
Selected Modification:		**z_{CoG} = 30.1 m**	
Parameter	**Repetition 2**	**Repetition 3**	Deviation
y_{CoG} (m)	*0*	*1.5*	*1.5*
Average (NRMSEs)	0.922	0.923	0.001
r_{yy} (m)	*52.1*	*56.7*	*4.6*
Pitch motion (NRMSE)	*0.605*	*0.961*	*0.356*
B_{visc} (4,4) (kNsm^2/m)	2.20E+06	1.12E+06	0.5* Orig.value
Roll motion (NRMSE)	0.958	0.960	0.002
Selected Modification:		**r_{yy} = 56.7 m**	
Parameter	**Repetition 3**	**Repetition 4**	**Deviation**
z_{CoG} (m)	30.1	28.9	-1.2
Average (NRMSEs)	0.982	0.992	0.010
Selected Modification:		**z_{CoG} = 28.9 m**	
Parameter	**Repetition 4**	**Repetition 5**	**Deviation**
r_{yy} (m)	56.7	57.3	0.6
Pitch motion (NRMSE)	0.960	0.995	0.035
B_{visc} (4,4) (kNsm^2/m)	2.20E+06	3.61E+06	1.6* Orig.value
Roll motion (NRMSE)	0.995	0.996	0.001
Selected Modification:		**r_{yy} = 56.7 m and B_{visc} (4,4) = 3.61E+06**	

The final NRMSEs of the vessel response spectra are presented in the following table:

Table 8: Final NRMSEs: Test case 1

Motions	NRMSE-Initial	NRMSE-Final
Surge	0.967	1.000
Sway	0.943	0.997
Heave	0.985	0.999
Roll	0.837	0.996
Pitch	0.281	0.995
Yaw	0.836	1.000
Average (NRMSEs)	0.808	0.998

As explained before, the response spectra of the given data set were obtained by making specific changes to the *standard* vessel properties. These changes are the *targets*. To validate the results of the calibration procedure, these targets should now be revealed and compared with the *identified* (*back-calculated*) properties. The identified and the target changes are compared in the following table.

Table 9: Final results: Test case 1

Quantity	Standard value	Identified value	Target value
r_{yy} **(m)**	52.1	57.3	57.3
r_{zz} **(m)**	52.1	54.7	54.7
z_{CoG} **(m)**	24.5	28.9	28.8
B_{visc}**(4,4) (kNsm²/m)**	2.20E+06	3.61E+06	4.40E+06

The deviations between the identified and the target values for the radii of gyration and the CoG position are within 0.8% of the original values respectively. Thus, the quantities r_{yy}, r_{zz} and z_{CoG} are identified with accuracy. However, the identified viscous damping for roll motion $B_{visc}(4,4)$ is 36% less than the target value.

In Figure 14, the response spectra based on the identified modifications and the given dataset are compared.

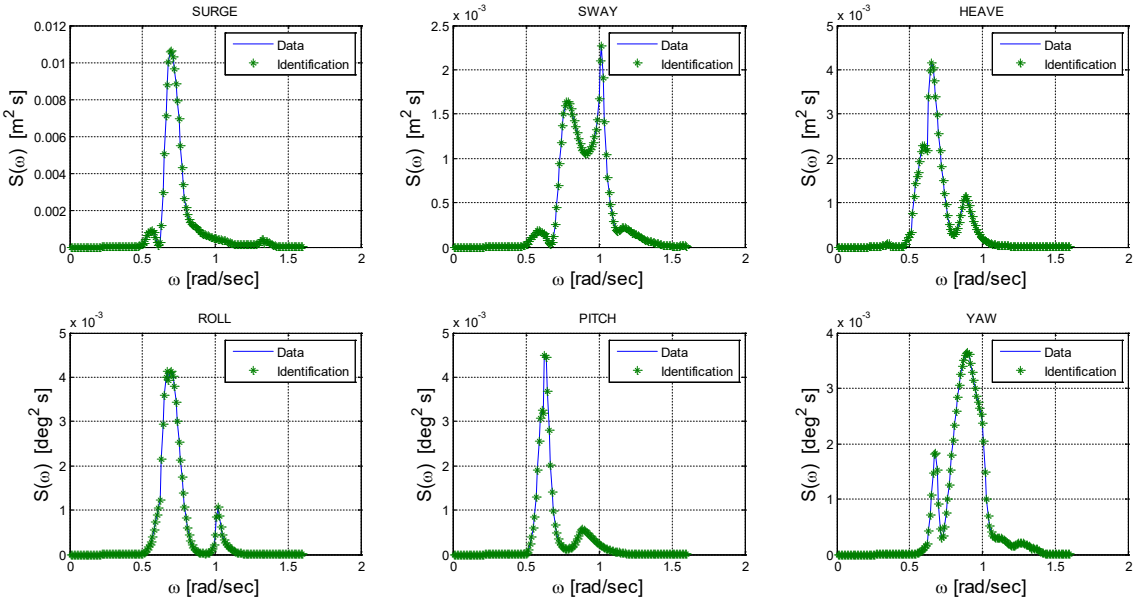

Figure 14: Comparison of *given* response spectra with spectra as calculated with *identified (back-calculated) RAOs*, Test case 1

Finally, the *target* and *back-calculated RAOs* are compared. In Figure 15 and Figure 16, the vessel RAOs for roll and pitch that show the most improvement have been depicted. In these figures the following RAOs are shown:

- *Back-calculated RAOs*: Specified as 'Identification-Results' (in green)
- *Standard RAOs*: Specified as 'Original' (in red)
- *Target RAOs*: Specified as 'Solution' (in blue)

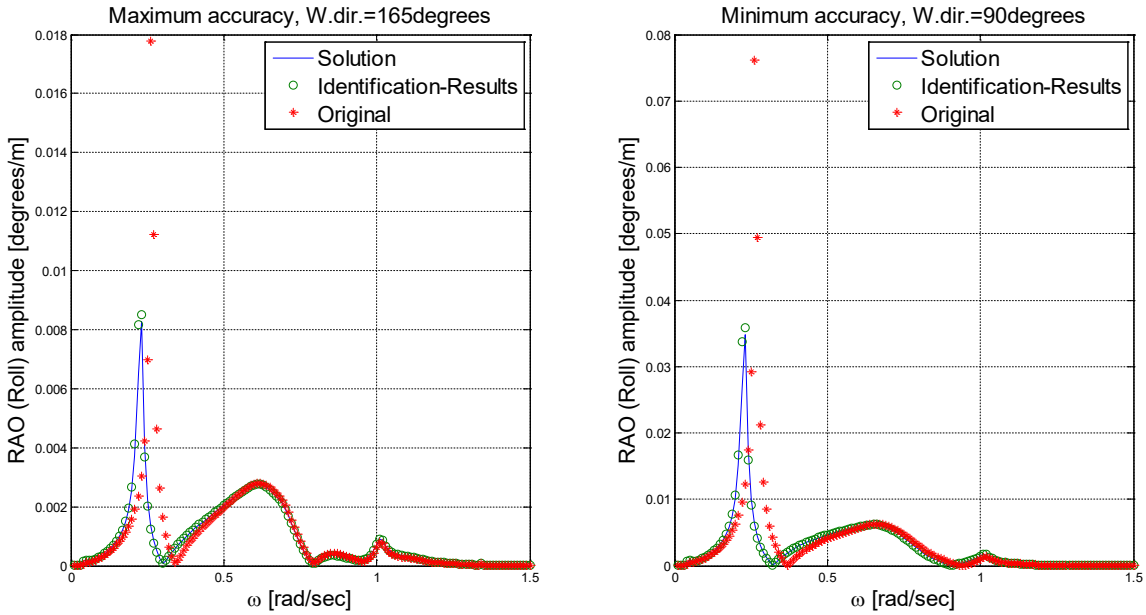

Figure 15: Roll-RAO, Amplitude, Test case 1

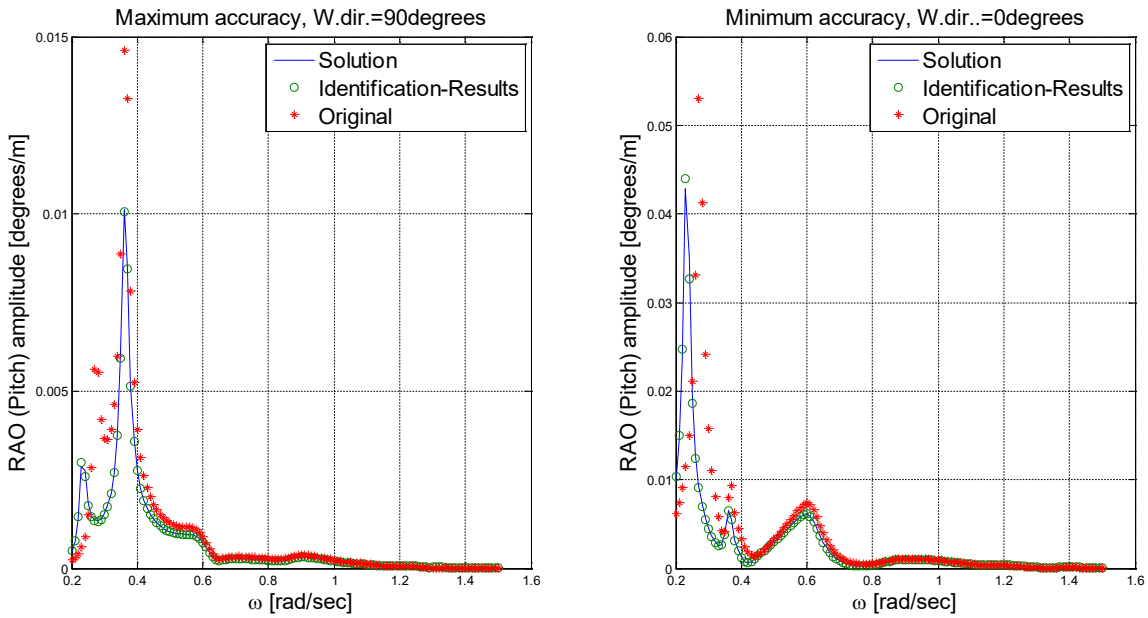

Figure 16: Pitch-RAO, Amplitude, Test case 1

The NRMSEs of the *standard RAOs* with respect to the *target RAOs* and the NRMSEs of the *back-calculated (identified) RAOs* with respect to the *target RAOs* are shown in Table 10.

Table 10: Comparison of NRMSEs of standard and identified RAOs: Test case 1

Surge-RAO	**Standard RAOs - Target RAOs**	**Identified RAOs - Target RAOs**
Average NRMSE (all wave dir.)	0.983	0.999
Minimum NRMSE	0.879 (directions: 90º)	0.996 (directions: 90º)
Maximum NRMSE	0.993 (directions: 45º)	1.000 (directions: 45º)
Sway-RAO	**Standard RAOs - Target RAOs**	**Identified RAOs - Target RAOs**
Average NRMSE (all wave dir.)	0.959	0.993
Minimum NRMSE	0.957 (directions: 90º)	0.993 (directions: 90º)
Maximum NRMSE	0.960 (directions: 15º)	0.994 (directions: 15º)
Heave-RAO	**Standard RAOs - Target RAOs**	**Identified RAOs - Target RAOs**
Average NRMSE (all wave dir.)	0.941	0.998
Minimum NRMSE	0.914 (directions: 180º)	0.996 (directions: 180º)
Maximum NRMSE	0.966 (directions: 90º)	1.000 (directions: 90º)
Roll-RAO	**Standard RAOs - Target RAOs**	**Identified RAOs - Target RAOs**
Average NRMSE (all wave dir.)	0.110	0.888
Minimum NRMSE	0.089 (directions: 90º)	0.880 (directions: 90º)
Maximum NRMSE	0.136 (directions: 165º)	0.897 (directions: 165º)
Pitch-RAO	**Standard RAOs - Target RAOs**	**Identified RAOs - Target RAOs**
Average NRMSE (all wave dir.)	0.220	0.957
Minimum NRMSE	0.132 (directions: 0º)	0.952 (directions: 0º)
Maximum NRMSE	0.562 (directions: 90º)	0.985 (directions: 90º)
Yaw-RAO	**Standard RAOs - Target RAOs**	**Identified RAOs - Target RAOs**
Average NRMSE (all wave dir.)	0.841	0.992
Minimum NRMSE	0.659 (directions: 90º)	0.982 (directions: 90º)
Maximum NRMSE	0.899 (directions: 15º)	0.997 (directions: 165º)

To conclude, the identified RAOs approximate the target RAOs of test case 1 with accuracy and therefore the vessel motion spectra are predicted with accuracy by the identified RAOs. For real-life situations, the identified RAOs would of course need to be tested against an additional set of measurements in a different seastate to ensure their practical usability.

5.2 Test case 2

The purpose of this test case is to investigate whether it is possible to calibrate the potential added mass, damping and wave forces. The vessel draught has been changed to 23.0 m. The vessel's displacement is now 110650 m^3 and the position of the CoG is [62.2, 0.0, 23.0]. The water plane area and radii of gyration are unchanged. The *target RAOs* have been determined based on a diffraction calculation performed in the normal manner using the new draught. With the *target RAOs* a data set of motion responses is generated. It will now be attempted to obtain the *target RAOs* on the bases of the given motion responses and the *standard RAOs* at the old draught.

The directional wave spectrum used in Test case 2 is depicted in Figure 17. The significant wave height of the spectrum is H_s = 1.6 m. The vessel is experiencing seas coming from the Eastsoutheast. The heading of the vessel is 40° (approximately Northeast).

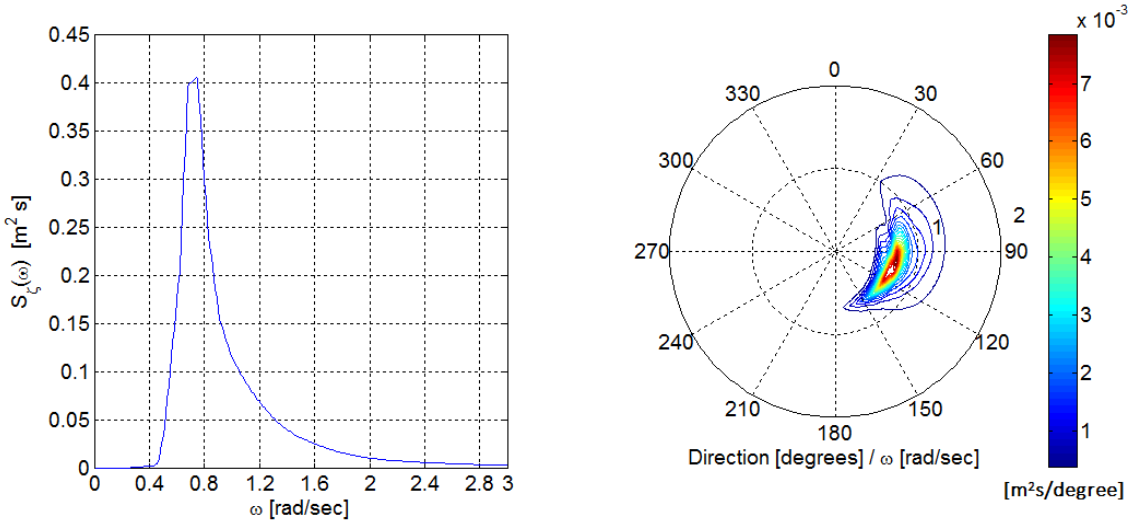

Figure 17: Wave spectrum used in Test case 2

With the *fitted standard* RAOs the vessel responses are calculated. The calculated motion spectra are compared with the spectra of the given data set in Figure 18. The initial NRMSEs for each of the vessel motions are as follows: surge = 0.847, sway = 0.777, heave = 0.852, roll = 0.694, pitch = 0.682, yaw = 0.863.

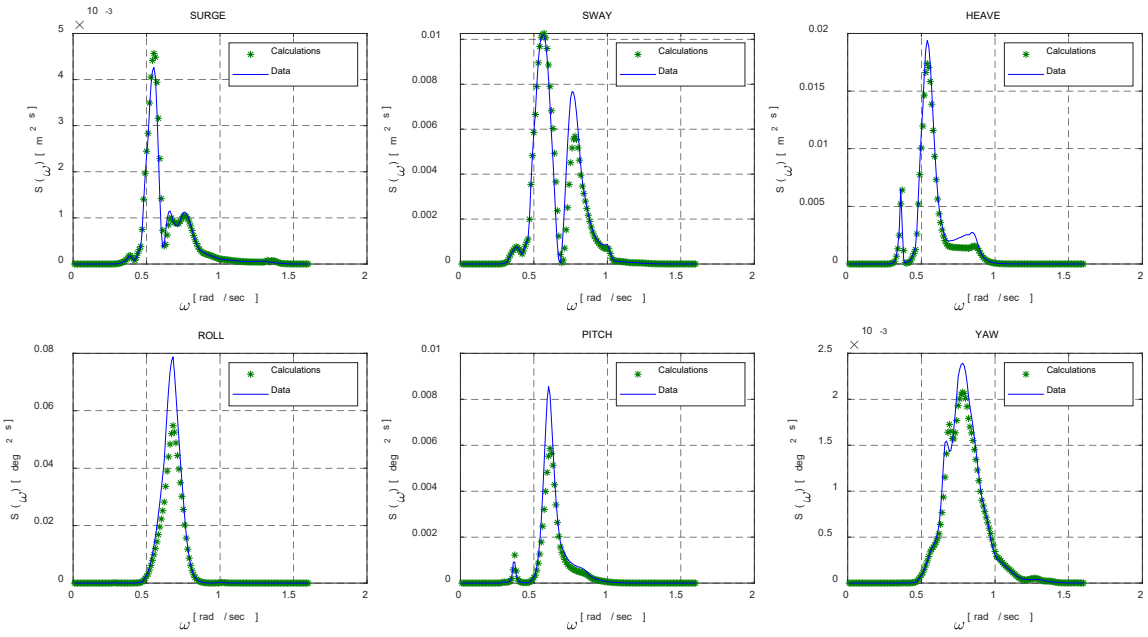

Figure 18: Comparison of *given* response spectra with spectra as calculated with *fitted standard RAOs*, Test case 2

The results of the calibration procedure for the potential mass, damping and wave forces are given below. The parameter *c* denotes the residues of the approximation functions.

Table 11: Calibration of residues of potential mass, damping and wave forces, Test case 2

Elements	New Values
c= 5-6 for F5(ω,150º)	-3.2016*Orig. Value
c= 5-6 for F4(ω,90º)	6.5623*Orig. Value
c= 9-10 for F2(ω,105º)	1.8115*Orig. Value
c= 5-6 for ab26	0.3291*Orig. Value
c= 13-14 for F6(ω,135º)	-1.8309*Orig. Value
c= 5-6 for ab15	0.0728*Orig. Value
c= 3-4 for ab55	0.3291*Orig. Value
c= 7-8 for F3(ω,150º)	8.6869*Orig. Value
c= 5-6 for F3(ω,90º)	1.0732*Orig. Value
c= 1-2 for ab55	-1.8421*Orig. Value
c= 11-12 for ab35	-0.0856*Orig. Value
c= 7-8 for F3(ω,105º)	-1.5967*Orig. Value
c= 35-36 for F2(ω,90º)	-5.7984*Orig. Value
c= 3-4 for F3(ω,75º)	-1.5967*Orig. Value
c= 7-8 for F2(ω,120º)	2.3131*Orig. Value
c= 17-18 for F2(ω,135º)	6.5623*Orig. Value
c= 3-4 for F5(ω,150º)	4.4377*Orig. Value

The resulting NRMSEs are given in the Table 12.

Table 12: Final NRMSEs, Test case 2

Motions	NRMSE-Initial	NRMSE-Final
Surge	0.847	0.956
Sway	0.777	0.903
Heave	0.852	0.937
Roll	0.694	0.949
Pitch	0.682	0.868
Yaw	0.863	0.933
Average (NRMSEs)	0.786	0.924

In Figure 19, the response spectra based on the identified modifications and the given dataset are compared.

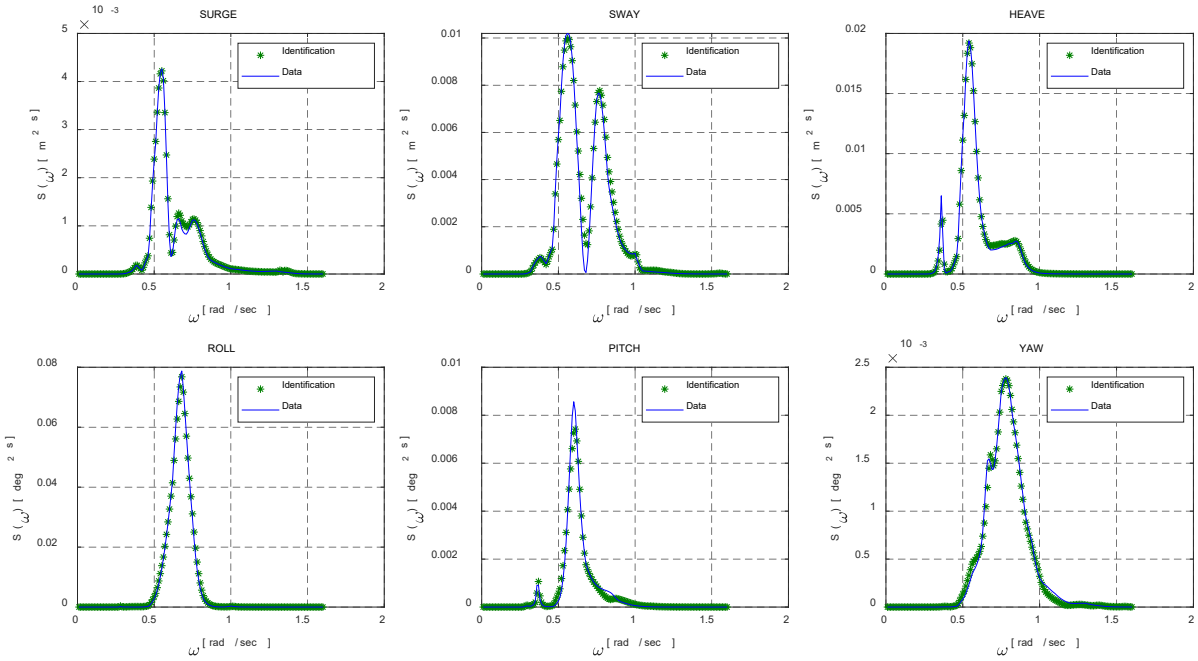

Figure 19: Comparison of *given* response spectra with spectra as calculated with *identified (back-calculated) RAOs*, Test case 2

In Figure 20, vessel RAOs for heave and roll of wave directions 180 and 120 degrees respectively are shown. These RAOs show the most improvement. In Figure 21, vessel RAOs for pitch and yaw of wave directions 150 and 135 degrees respectively are shown. These RAOs show the least improvement. As before, in these figures the following RAOs are shown:

- *Back-calculated RAOs*: Specified as 'Identification TC2' (in green)
- *Standard RAOs*: Specified as 'Original' (in red)
- *Target RAOs*: Specified as 'Solution' (in blue)

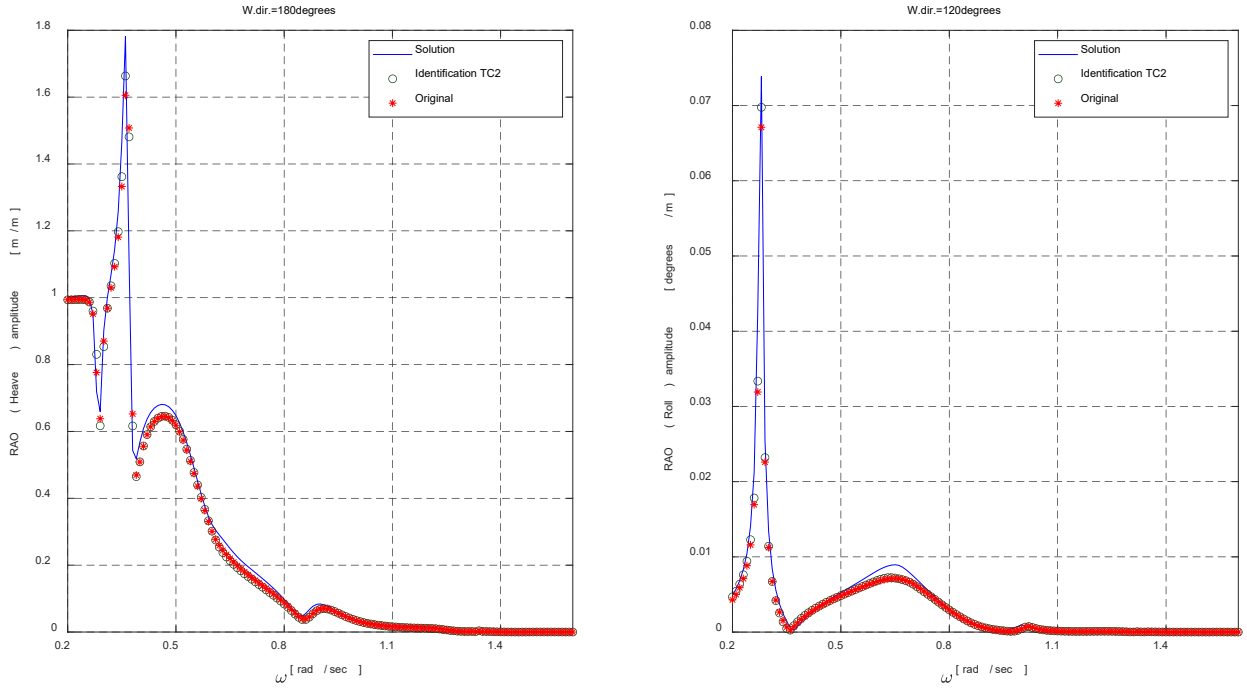

Figure 20: Amplitude of Heave-RAO, Roll-RAO, Test case 2

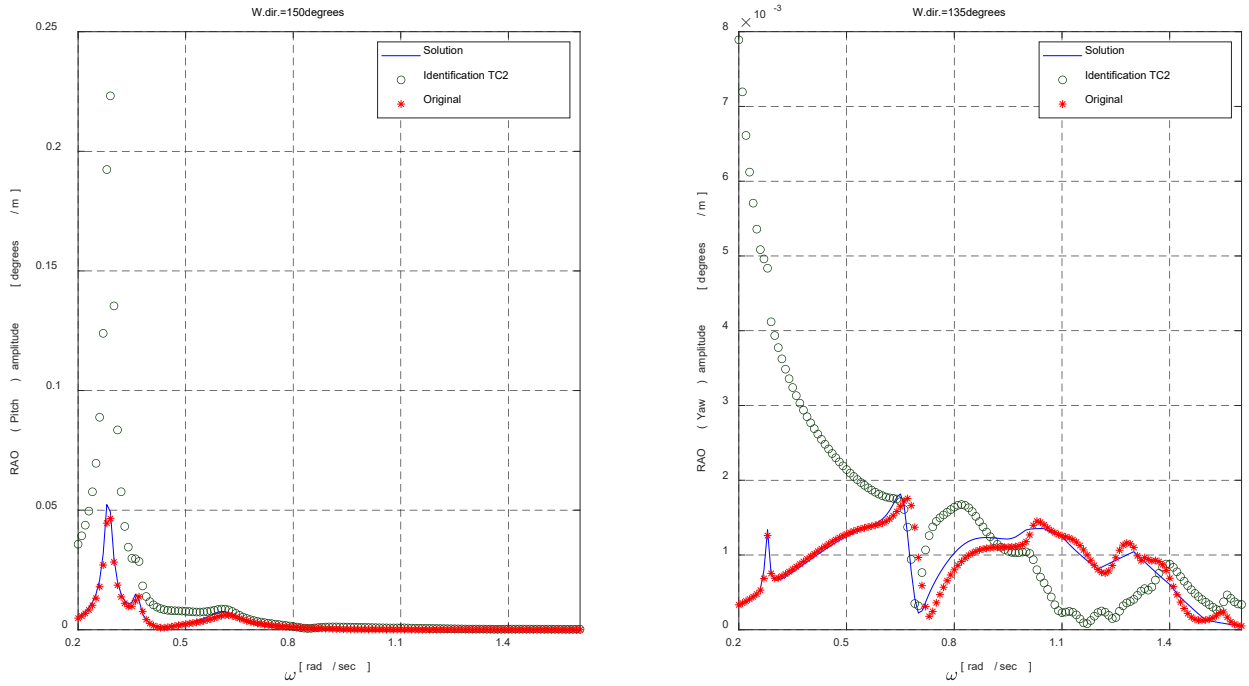

Figure 21: Amplitude of Pitch-RAO, Yaw-RAO, Test case 2

The NRMSEs of the *standard RAOs* with respect to the *target RAOs* and the NRMSEs of the *back-calculated (identified) RAOs* with respect to the *target RAOs* are shown in Table 13.

Table 13: Comparison of NRMSEs of standard and identified RAOs: Test case 2

Surge-RAO	**Standard RAOs - Target RAOs**	**Identified RAOs - Target RAOs**
Average NRMSE (all wave dir.)	0.925	0.925
Minimum NRMSE	0.765 (directions: 90°)	0.719 (directions: 90°)
Maximum NRMSE	0.952 (directions: 165°)	0.966 (directions: 165°)
Sway-RAO	**Standard RAOs - Target RAOs**	**Identified RAOs - Target RAOs**
Average NRMSE (all wave dir.)	0.955	0.924
Minimum NRMSE	0.922 (directions: 15°)	0.794 (directions: 90°)
Maximum NRMSE	0.969 (directions: 150°)	0.968 (directions: 150°)
Heave-RAO	**Standard RAOs - Target RAOs**	**Identified RAOs - Target RAOs**
Average NRMSE (all wave dir.)	0.862	0.819
Minimum NRMSE	0.831 (directions: 90°)	0.484 (directions: 105°)
Maximum NRMSE	0.893 (directions: 0°)	0.899 (directions: 180°)
Roll-RAO	**Standard RAOs - Target RAOs**	**Identified RAOs - Target RAOs**
Average NRMSE (all wave dir.)	0.811	0.786
Minimum NRMSE	0.793 (directions: 165°)	0.515 (directions: 90°)
Maximum NRMSE	0.823 (directions: 75°)	0.850 (directions: 120°)
Pitch-RAO	**Standard RAOs - Target RAOs**	**Identified RAOs - Target RAOs**
Average NRMSE (all wave dir.)	0.845	0.732
Minimum NRMSE	0.817 (directions: 75°)	0.210 (directions: 150°)
Maximum NRMSE	0.859 (directions: 135°)	0.841 (directions: 135°)
Yaw-RAO	**Standard RAOs - Target RAOs**	**Identified RAOs - Target RAOs**
Average NRMSE (all wave dir.)	0.771	0.602
Minimum NRMSE	0.681 (directions: 165°)	0.017 (directions: 135°)
Maximum NRMSE	0.877 (directions: 75°)	0.828 (directions: 60°)

In general, the modifications as determined by the calibration procedure result in more accurate response spectra. The resulting NRMSEs are satisfying. However, the resulting *back-calculated RAOs* differ from the *target RAOs*.

It is interesting to note that, in Figure 20 and Figure 21, the largest errors occur at low frequencies, where there is little energy in the wave spectrum. See Figure 17. It should be clear that, if part of a RAO is not addressed by the wave climate, it is simply not possible to infer any information on the RAO in that frequency range from the measured vessel responses.

5.3 Test case 3

The purpose of this test case is to investigate whether the *target RAOs* could still be identified in different wave conditions and by using the *back-calculated RAOs* of Test case 2 as *standard RAOs*. The *target RAOs* are the same as in test case 2. With the *target RAOs* a data set of motion responses is generated by applying a new wave spectrum. It will now be attempted to obtain the *target RAOs* on the bases of the given motion responses and the *back-calculated RAOs* of test case 2.

The directional wave spectrum used in Test case 3 is depicted in Figure 22. Note that both the frequency content and directions of the new spectrum are different from that in test case 2. The vessel is experiencing seas coming from the Westsouthwest. The heading of the vessel is 40° (approximately Northeast).

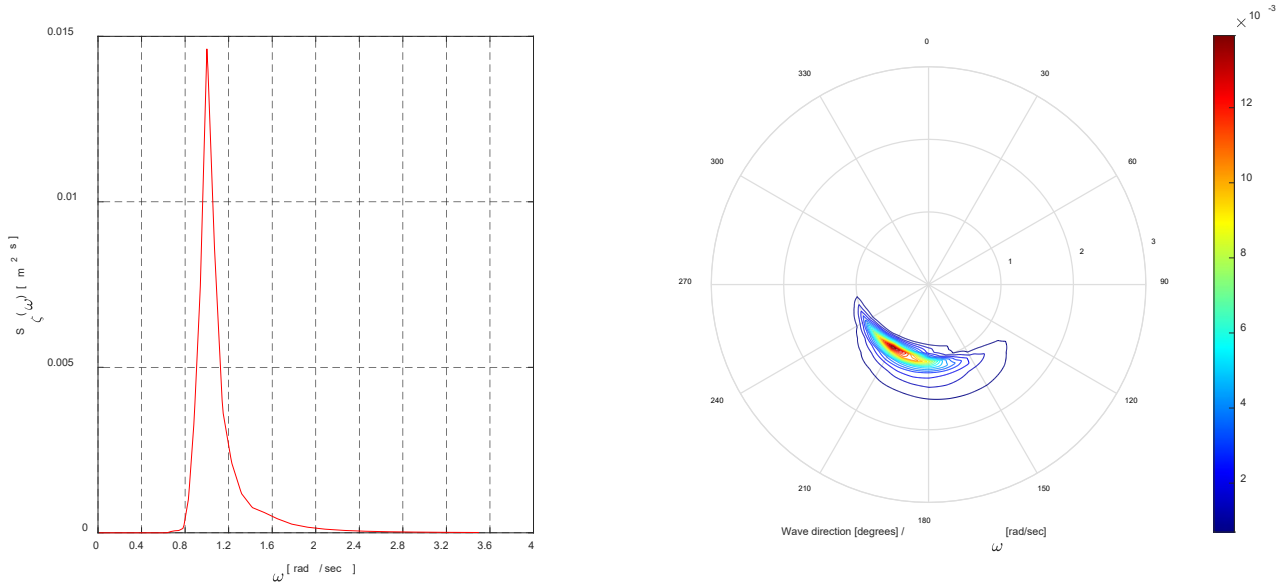

Figure 22: Wave spectrum used in Test case 3

Applying the new wave spectrum and using the *back-calculated RAOs* of Test case 2 and the *target* RAOs, the new vessel responses are calculated: The responses specified as *'Identification TC2'* are based on the *back-calculated RAOs* of Test case 2 and the responses specified as *'New Data'* are based on the *target* RAOs. The motion spectra are compared in Figure 23. The NRMSEs for each of the vessel motions are as follows: surge = 0.863, sway = 0.535, heave = 0.708, roll = 0.465, pitch = 0.785, yaw = 0.915. As it is shown from the values of the NRMSEs, the vessel responses in different wave conditions do not show a good agreement.

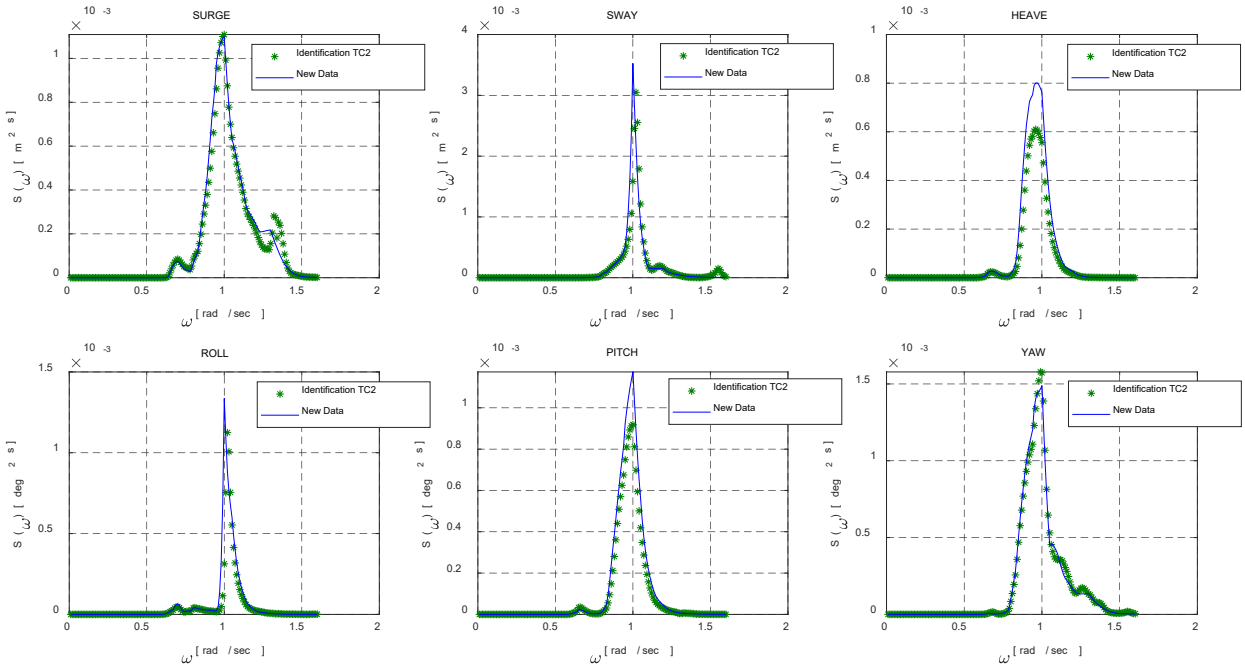

Figure 23: Comparison of response spectra as calculated with *back-calculated RAOs* of Test case 2 and *target* RAOs with new wave spectrum, Test case 3

The results of the calibration procedure for the potential mass, damping and wave forces are given below. The parameter *c* denotes the residues of the approximation functions. In

comparison to test case 2, the predicted modifications of test case 3 for the wave forces refer to different wave directions.

Table 14: Calibration of residues of potential mass, damping and wave forces, Test case 3

Elements	New Values
c= 5-6 for F5(ω,150°)	-3.2016*Orig. Value
c= 5-6 for F4(ω,90°)	6.5623*Orig. Value
c= 9-10 for F2(ω,105°)	1.8115*Orig. Value
c= 5-6 for ab26	0.3291*Orig. Value
c= 13-14 for F6(ω,135°)	-1.8309*Orig. Value
c= 5-6 for ab15	0.0728*Orig. Value
c= 3-4 for ab55	0.3291*Orig. Value
c= 7-8 for F3(ω,150°)	8.6869*Orig. Value
c= 5-6 for F3(ω,90°)	1.0732*Orig. Value
c= 1-2 for ab55	-1.8421*Orig. Value
c= 11-12 for ab35	-0.0856*Orig. Value
c= 7-8 for F3(ω,105°)	-1.5967*Orig. Value
c= 35-36 for F2(ω,90°)	-5.7984*Orig. Value
c= 3-4 for F3(ω,75°)	-1.5967*Orig. Value
c= 7-8 for F2(ω,120°)	2.3131*Orig. Value
c= 17-18 for F2(ω,135°)	6.5623*Orig. Value
c= 3-4 for F5(ω,150°)	4.4377*Orig. Value

The resulting NRMSEs are given in the Table 15.

Table 15: Final NRMSEs, Test case 3

Motions	NRMSE-Initial	NRMSE-Final
Surge	0.863	0.887
Sway	0.535	0.833
Heave	0.708	0.972
Roll	0.465	0.807
Pitch	0.785	0.947
Yaw	0.915	0.956
Average (NRMSEs)	0.712	0.900

In Figure 24 the response spectra based on the identified modifications of test case 3 and the new dataset are compared.

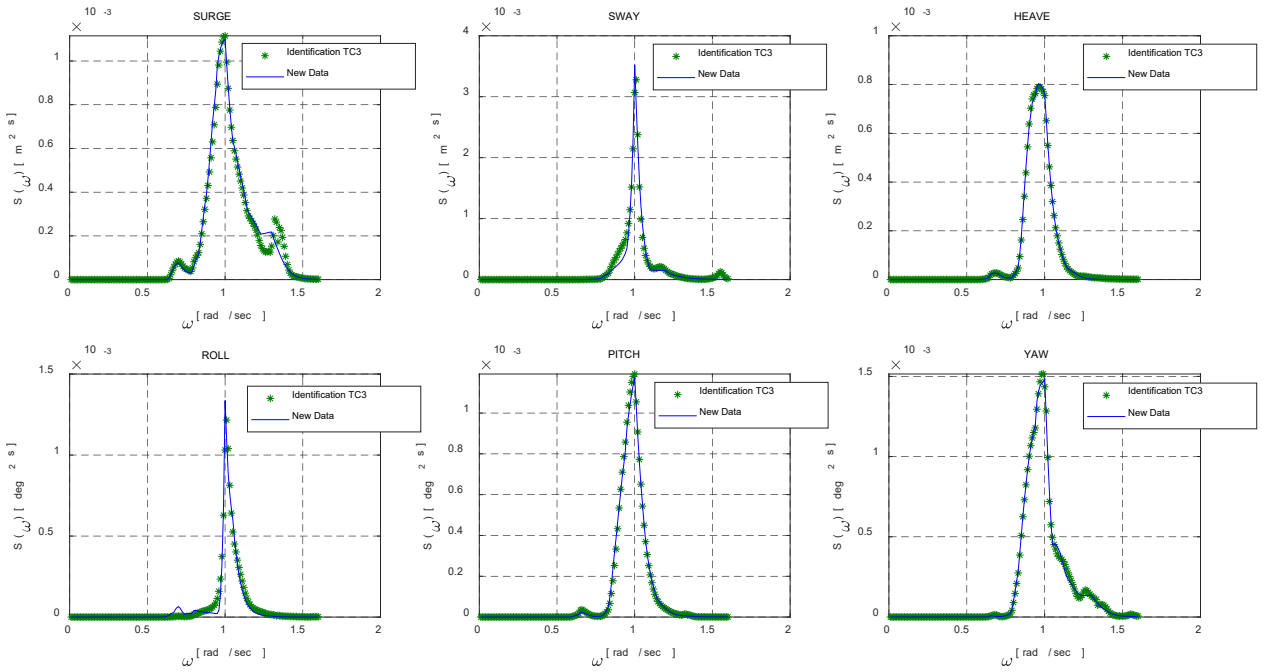

Figure 24: Comparison of new response spectra based on *target* RAOs with spectra as calculated with new *identified (back-calculated) RAOs*, Test case 3

In Figure 25, vessel RAOs for heave and surge of wave directions 180 and 165 degrees respectively are shown. These RAOs show the most improvement. In Figure 26, vessel RAOs for yaw of wave directions 15 and 30 degrees are shown. These RAOs show the least improvement. In these figures the following RAOs are shown:

- *Back-calculated RAOs* of test case 3: Specified as 'Identification TC3' (in green)
- *Back-calculated RAOs* of test case 2: Specified as 'Identification TC2' (in red)
- *Target RAOs*: Specified as 'Solution' (in blue)

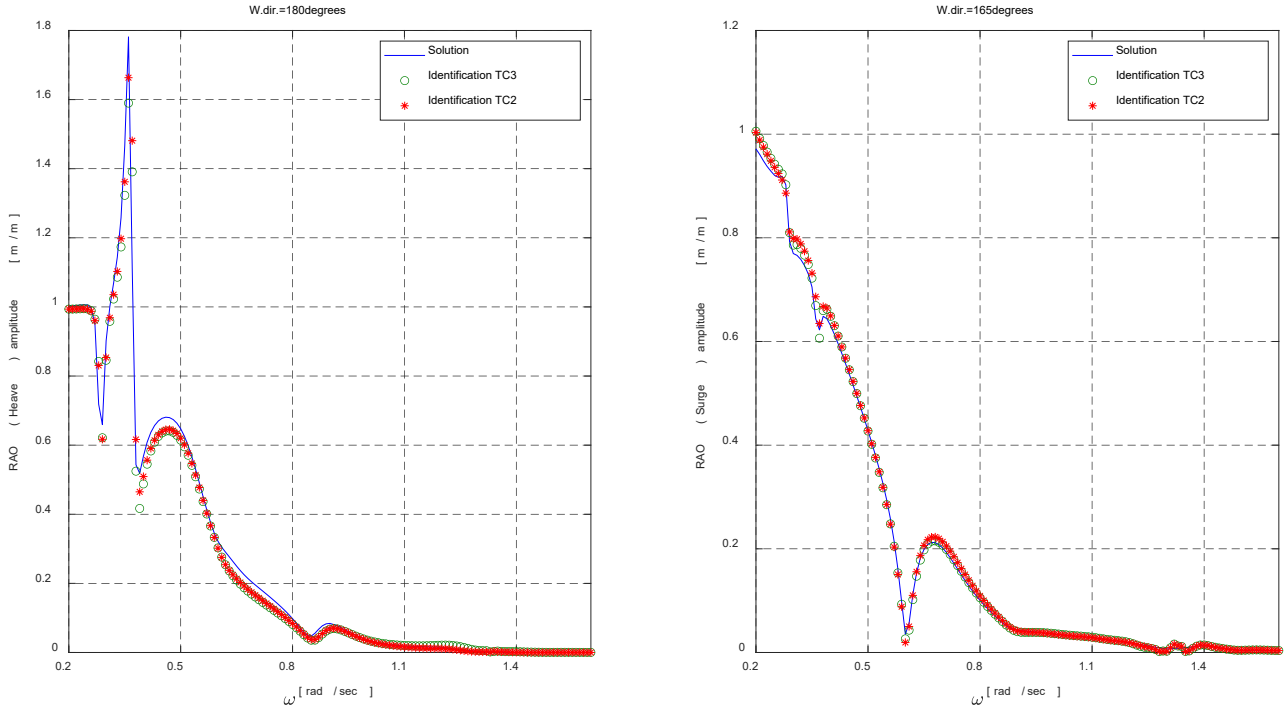

Figure 25: Amplitude of Heave-RAO, Surge-RAO, Test case 3

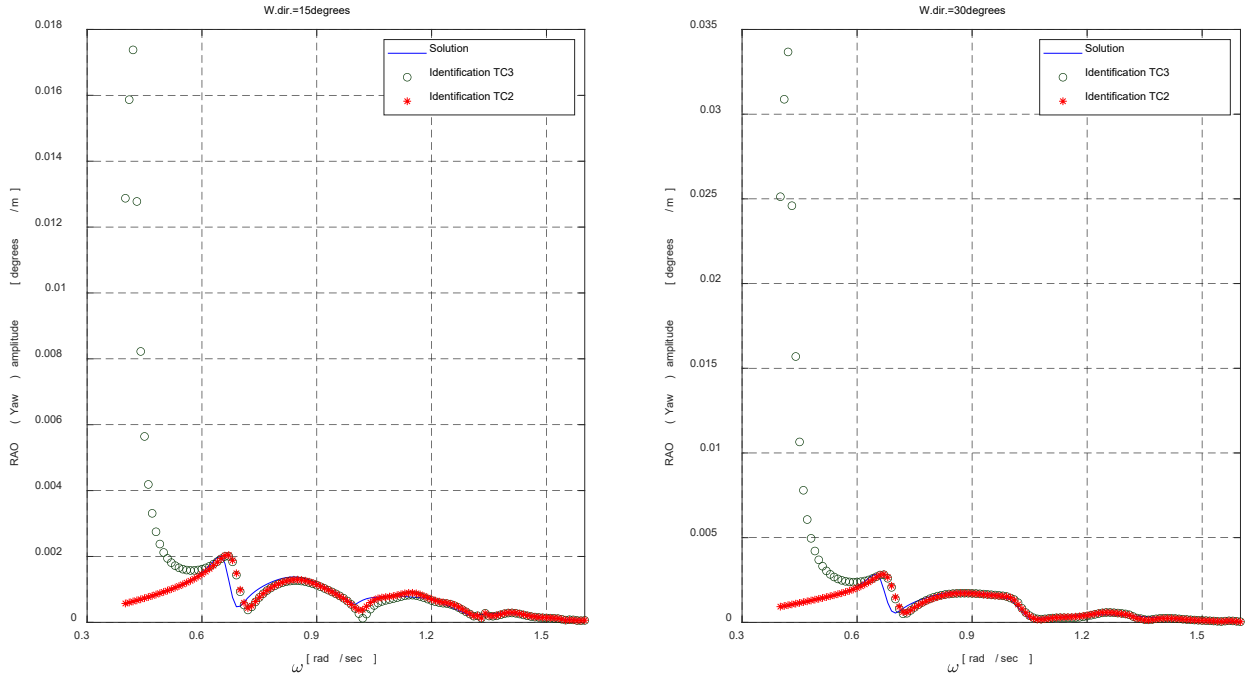

Figure 26: Amplitude of Yaw-RAO, Test case 3

The NRMSEs between the *standard RAOs*, the *target RAOs*, the *back-calculated RAOs* of test case 2 and the *back-calculated RAOs* of test case 3 are shown in the following table.

Table 16: Comparison of NRMSEs: Test case 3

Surge-RAO	**Standard RAOs - Target RAOs**	**Identified RAOs TC2 - Target RAOs**	**Identified RAOs TC3 - Target RAOs**
Average NRMSE	0.925	0.925	0.900
Minimum NRMSE	0.765 (directions: 90º)	0.719 (directions: 90º)	0.651 (directions: 90º)
Maximum NRMSE	0.952 (directions: 165º)	0.966 (directions: 165º)	0.971 (directions: 165º)
Sway-RAO	**Standard RAOs - Target RAOs**	**Identified RAOs TC2 - Target RAOs**	**Identified RAOs TC3 - Target RAOs**
Average NRMSE	0.955	0.924	-0.011
Minimum NRMSE	0.922 (directions: 15º)	0.794 (directions: 90º)	-0.018 (directions: 15º)
Maximum NRMSE	0.969 (directions: 150º)	0.968 (directions: 150º)	-0.007 (directions: 30º)
Heave-RAO	**Standard RAOs - Target RAOs**	**Identified RAOs TC2 - Target RAOs**	**Identified RAOs TC3 - Target RAOs**
Average NRMSE	0.862	0.819	0.785
Minimum NRMSE	0.831 (directions: 90º)	0.484 (directions: 105º)	0.116 (directions: 15º)
Maximum NRMSE	0.893 (directions: 0º)	0.899 (directions: 180º)	0.897 (directions: 180º)
Roll-RAO	**Standard RAOs - Target RAOs**	**Identified RAOs TC2 - Target RAOs**	**Identified RAOs TC3 - Target RAOs**
Average NRMSE	0.811	0.786	0.042
Minimum NRMSE	0.793 (directions: 165º)	0.515 (directions: 90º)	0.018 (directions: 15º)
Maximum NRMSE	0.823 (directions: 75º)	0.850 (directions: 120º)	0.051 (directions: 75º)
Pitch-RAO	**Standard RAOs - Target RAOs**	**Identified RAOs TC2 - Target RAOs**	**Identified RAOs TC3 - Target RAOs**
Average NRMSE	0.845	0.732	0.681
Minimum NRMSE	0.817 (directions: 75º)	0.210 (directions: 150º)	0.190 (directions: 15º)
Maximum NRMSE	0.859 (directions: 135º)	0.841 (directions: 135º)	0.820 (directions: 120º)
Yaw-RAO	**Standard RAOs - Target RAOs**	**Identified RAOs TC2 - Target RAOs**	**Identified RAOs TC3 - Target RAOs**
Average NRMSE	0.771	0.602	-0.030
Minimum NRMSE	0.681 (directions: 165º)	0.017 (directions: 135º)	-0.035 (directions: 15º)
Maximum NRMSE	0.877 (directions: 75º)	0.828 (directions: 60º)	-0.025 (directions: 30º)

As shown in Table 16 the identified modifications of test case 3 do not lead to accurate prediction of the *target RAOs*. However, the vessel responses as determined by the calibration procedure again show a good agreement. By comparing the identified modifications of test case 2 and 3 no pattern can be found that leads to accurate prediction of RAOs. This is because a large number of combinations of modified elements can be found that results in matching vessel motion spectra. That verifies the non-uniqueness of the solution when a large number of parameters needs to be adjusted such as the potential added mass, damping and wave forces.

6 CONCLUSIONS

A method for calibrating existing RAOs based on measured ship motions and wave spectra has been proposed. The method consists of two steps, namely a) a vector fitting procedure for representing the frequency dependent hydrodynamic properties using only a limited number of parameters, and b) identification algorithms for identifying these and other unknown parameters of the RAOs from measured data.

It is shown that the frequency dependent hydrodynamic added mass and damping can be approximated with accuracy by a ratio of two polynomials using the vector fitting method. The accuracy of the fitting process is lower for the wave forces, but the results are still satisfying. Additionally, the vector fitting method allows for an interpolation of the wave forces over the wave directions. The accuracy of the fitting process was also tested by calculating the response spectra and RAOs using the approximation functions. At very low frequencies some of the fitted curves of the RAOs were found to contain inaccuracies. Since, however, the swell and wind seas occur at higher frequencies, these inaccuracies do not influence the final response spectra.

The main characteristic of the developed identification algorithms is that each parameter of the RAOs is investigated separately. It was shown to be important to select only a certain amount of elements to calibrate based on logical criteria, e.g. the potential added mass, damping and wave forces should be investigated for a change of draught or when there are known inaccuracies at an inconvenient draught. For standard draughts where the pontoons of semi-submersible vessels are below the sea surface, only the radii of gyration, the CoG position and viscous roll damping need to be adjusted. In case of semi-submersibles, large changes in viscous damping are not realistic, thus the identification method should focus on the calibration of the radii of gyration and the CoG position. When the identification method is applied to hull-geometry ships, then the investigation of viscous roll damping would have an important impact on the motion responses.

To conclude, the proposed methodology was shown to be able to identify RAOs with accuracy in situations where the initial discrepancies were caused by errors in the vessel's radii of gyration, center of gravity, or viscous damping. When the errors are related to the potential mass, damping and wave forces, however, the non-uniqueness of the solution becomes prohibitive. The number of unknowns, in terms of potential mass, damping and wave forces, is simply too high in comparison with the number of available equations. Therefore a large number of combinations of parameter modifications can lead to accurate response spectra but not to accurate RAOs. Nevertheless, the identified modifications can be used as sets of 'pseudo-coefficients' that are able to, in certain situations, *predict the vessel response* much more accurately than standard radiation-diffraction codes.

7 REFERENCES

[1] C.-H. Lee. Wamit theory manual. Report No. 95-2. Cambridge. Massachusettes institute of technology, Department of ocean engineering. October 1995.

[2] MOSES Technical Information.
http://bentley.ultramarine.com/hdesk/document/document.htm

[3] O.M. Faltinsen. Sea Loads on Ships and Offshore Structures. Cambridge University Press. 1990.

[4] J.N. Newman. Efficient hydrodynamic analysis of very large floating structures. Marine Structures. 2005. Vol. 18, 169-180.

[5] J.M.J. Journée, W.W. Massie. Offshore Hydromechanics. Delft University of Technology. 2001.

[6] B. Iwanowski, M. Lefranc, R. Wemmenhove. CFD Simulation of Wave Run-up on a Semi-Submersible and Comparison with Experiment. Proceedings of the ASME 2009 28th International Conference on Ocean, Offshore and Arctic Engineering. 2009.

[7] R de Bruijn, F. Huijs, T. Bunnik, R. Huijsmans, M. Gerritsma. Calculation of Wave Forces and Internal Loads on a Semi-Submersible at Shallow Draft Using an iVOF Method. Proceedings of the ASME 2011 30th International Conference on Ocean, Offshore and Arctic Engineering. 2011.

[8] H. Ottens, A. Pistidda. Motion RAOs of a SSCV at Deep and Inconvenient Draft Using CFD. Proceedings of the ASME 2015 34th International Conference on Ocean, Offshore and Arctic Engineering. 2015.

[9] A.R.J.M. Lloyd. Seakeeping: Ship Behaviour in Rough Weather. Seakeeping. 1998.

[10] N. Tanaka. A Study on the Bilge Keels (Part 4 – On the eddy making resistance to the rolling of a ship hull). JSNAJ. 1960.

[11] J. Falzarano, A. Somayajula, R. Seah. An Overview of the Prediction Methods for Roll Damping of Ships. Ocean Systems Engineering. Vol. 5 No. 2, 55-76. 2015.

[12] S.K. Chakrabarti. Pros and cons of transient waves. Applied Ocean Research 17, 91-92. 1995.

[13] P. Roux de Reilhac, F. Bonnefoy, J.M. Rousset, P. Ferrant. Improved transient water wave technique for the experimental estimation of ship responses. Journal of fluids and structures 27, 456–466. 2011.

[14] D.E. Newland. An Introduction to Random Vibrations and Spectral Analysis. Longman Scientific & Technical. 1984.

[15] Adam Semlyen & Bjorn Gustavsen. Rational approximation of frequency domain responses by vector fitting. IEEE Transaction on Power Delivery. July 1999. Vol 14, p. 1052, No. 3.

[16] L. Bergdahl. Wave-Induced Loads and Ship Motions. Department of Civil and Environmental Engineering. Chalmers University of Technology. 2009. Report No. 2009:1.

[17] F. Liu, H. Lu, C. Ji .A general frequency-domain dynamic analysis algorithm for offshore structures with asymmetric matrices. Ocean Engineering. 2016. Vol. 125, 272-284.

[18] F. Liu, J. Chen, H. Qin. Frequency response estimation of floating structures by representation of retardation functions with complex exponentials. Marine Structures. 2017. Vol. 54, 144-166.

[19] J. Kotik and V. Mangulis. On the Kramers-Kronig relations for ship motions. International Shipbuilding Progress. 1962. 9:97, 361-368.

[20] 1994-2015 The MathWorks Inc. Goodness of fit between test and reference data. http://nl.mathworks.com/help/ident/ref/goodnessoffit.html#zmw57dd0e33974.

[21] W.H. Press, S.A. Teukolsky, W.T. Vetterling, Brian P. Flannery. Numerical Recipes in C. Second edition. Cambridge University Press. June 1992.

[22] E.B. Malta, R.T. Gonçalves, F.T. Matsumoto, F.R. Pereira, A.L.C. Fujarra and K. Nishimoto. Damping coefficient analyses for floating offshore structures. Proceedings of the ASME 2010 29th International Conference on Ocean, Offshore and Arctic Engineering. 2010